2010

Sensitivity of Planetary Boundary Layer to Varying Volumetric Soil Moisture: A Mesoscale Models Comparision

Asrid Suarez Gonzalez
Western Kentucky U

SENSITIVITY OF PLANETARY BOUNDARY LAYER TO VARYING VOLUMETRIC SOIL MOISTURE: A MESOSCALE MODELS COMPARISON

A Capstone Experience/Thesis Project

Presented in Partial Fulfillment of the Requirements for

The Degree Bachelor of Science with

Honors College Graduate Distinction at Western Kentucky University

By

Astrid Suarez Gonzalez

* * * * *

Western Kentucky University

2010

CE/T Committee:

Approved by

Professor Rezaul Mahmood, Advisor

Professor Gregory Goodrich _____

Advisor

Professor James Baker Department of Geography and Geolo

ABSTRACT

A comparison between two Mesoscale models, Colorado State University Regional Atmospheric Model System (RAMS) version 4.4 coupled with the Land-Ecosystem–Atmosphere Feedback Model (LEAF2) and Penn State/NCAR's Mesoscale Model (MM5) coupled with NOAH Land Surface Model, was conducted in order to assess the sensitivity of forecasted boundary layer variables to anomalous volumetric soil moistures. The study elaborates on the findings of Quintanar et al. (2008) using the study's experimental design as a template for our numerical model comparison. The experiments were conducted using the same synoptic events examined by Quintanar et al. (2008): June 11, June 17 and June 22, 2006. For each event, six simulations were conducted with RAMS and MM5 in which volumetric soil moisture was increase and decreased by 0.05, 0.10, and 0.15 m^3m^{-3}. The simulations were initialized with 1x1 degree FNL-Reanalysis data and a horizontal grid resolution of 12km. Each resulting simulation was individually analyzed. Overall, RAMS simulations presented a greater sensitivity and variability when forecasting precipitation and PBL parameters. Both models were able to capture the distribution and accumulation of precipitation with respect to NARR for the CTRL runs. However, during the sensitivity studies, RAMS fails to accurately position precipitation and other parameters such as equivalent potential temperature and vertical wind.

Keyword: soil moisture, planetary boundary layer, RAMS, MM5, land surface models

Dedicated to my friends and family

ACKNOWLEDGEMENTS

This project would not have been possible without the help and support of Dr. Rezaul Mahmood and Dr. Arturo I. Quintanar. Special help was also received from Dr. Adriana Beltran-Przekurat, Dr. Gregory Goodrich, and Mr. John Baker. Funding for this project was provided by a USDA Grant: #58-6445-6-068. This work has also benefited from a NOAA Grant: #NA06NWS4670010.

VITA

July 28, 1986 ……..Born – Guines, La Habana, Cuba

2006 ……..……...Fern Creek Traditional High School,
Louisville, Kentucky

2007-2008……..NSF Louis Strokes Scholarship Recipient

2009……NSF REU, University of Oklahoma, Norman, OK

2008-Present…… Kentucky Climate Center, Bowling Green, KY

FIELDS OF STUDY

Major Field: Meteorology

Minor Field: Mathematic

TABLE OF CONTENTS

LIST OF FIGURES

CHAPTER 1

INTRODUCTION

The sensitivity of planetary boundary layer (referred to as PBL herein) parameters to varying conditions of soil moisture (referred to as SM herein) has become the focus of attention of many numerical modeling studies dealing with short-term, regional, land-atmosphere processes (e.g. Houser et al. 1998; Fennessy and Shukla 1999; Douville et al. 2001; Findell and Eltahir 2003; and Quintanar et al. 2008). Perturbations of SM have been shown to affect the response of numerical models when forecasting boundary layer parameters such as evapotranspiration rates, Bowen ratio (ratio between sensible and latent heat fluxes), convective precipitation, vertical winds, and equivalent potential temperature (θ_e herein) (e.g. Beljaar et al. 1996; Eltahir 1998; Findell and Eltahir 2003; and Quintanar et al. 2008). Numerous techniques have been used in order to provide improved simulation of land-atmosphere interactions and the evolution of the PBL (e. g. Fennessy and Shukla 1999; Schlosser and Milly 2002; Weaver 2004; and Santanello et al. 2007).

Numerical experiments set in early spring and summer have revealed that increases in SM enhance the availability of water vapor throughout the PBL, the probabilities of clouds and convection, due to the increase of moist static stability (Eltahir 1998; Quintanar et al. 2008). On the contrary, under dryer conditions most of the incoming solar radiation is partitioned into sensible heat flux. Large Bowen ratios are conducive of thermal turbulences and convection, which can homogenize and deepen the PBL improving the potential for cloud formation (Ek and Mahrt 1994, Ek and Holstag 2004).

Recent modeled land-atmospheric interaction studies have revealed that 3-dimensional wind plays a more important role in convection inhibition and suppression that previously thought (Quintanar et al. 2008). Although soil-moisture-induced circulations are not likely to produce heavy precipitation (Baker et al. 2001), sharp horizontal gradients of moisture have been shown to produce turbulence and land sea breezes (Oockuchi et al. 1984). It has also been shown that strong backing winds or unidirectional winds with strong vertical shear can suppress convective processes. On the other hand, moderate veering through the atmosphere has been shown to enhance convection. Although the effect of SM on low level winds has only been addressed by a limited number of studies (e.g.

Oockuchi et al. 1984; Sutton et al. 2006); recent experiments have shown that significant drying of the environment can enhance the probability of veering winds patterns with vertical speeds of up to 10 ms^{-1}, thus enhancing the atmosphere convective potential (Quintanar et al. 2008).

Recently, Quintanar el al. (2008) conducted a MM5-based study (http://www.mmm. ucar.edu/mm5/mm5-home) in which perturbations of the initial conditions of SM resulted in variations of the precipitation patterns, Bowen ratio, vertical velocities, and equivalent potential temperature. In the study, Quintanar el al. (2008) examined three synoptic events with varying synoptic forcing occurring on June, 2006. Several single-deterministic simulations were conducted in which SM was increased and decreased by 0.05, 0.10 and 0.15 m^3m^{-3}. The simulations were individually examined. Three-member wet and dry ensembles were constructed and analyzed with respect to control runs for each study period. Quintanar et al. (2008) suggested that vertical velocities and equivalent potential temperature were good indicative of precipitation. While small Bowen ratio was needed, it was not a sufficient indicative to forecast precipitation. Quintanar et al. (2008) showed that decreases of SM were conducive of decreased precipitation. On the other hand, wet experiments increased precipitation slightly,

but less than anticipated.

Here, a comparative study is conducted in order to examine the response of PBL to changes in SM using MM5 and Regional Atmospheric Modeling System (RAMS) (Pielke et al. 1992; Cotton et al. 2003) version 4.4 (refer to as RAMS herein). MM5 and RAMS have been widely used for the examination of land-atmospheric interactions, due to their sophisticated land surface models (e.g. Weaver 2004; Pitman et al. 2004; Douglas et al. 2008; Quintanar et al. 2008; Quintanar et al. 2009). A limited number of studies have attempted to assess the efficacy of each model when forecasting various PBL processes (e. g. Cox et al. 1998; Patra et al. 2000; Zhong and Fast 2003). Cox et al. (1998) conducted a study in which four state-of-the-art atmospheric models were compared for nine climate "theater" throughout the globe. The study included RAMS, MM5, Navy Operational Regional Atmospheric Prediction System (NORAPS), and Relocatable Window Model (RWM) (Cox et al. 1998). Cox et al. (1998) found that the RAMS performed marginally ahead of MM5, with a slight statistical advantage. Zhong and Fast (2003) showed, through a multi-model intercomparison of RAMS, MM5 and Meso-Eta, that RAMS and MM5 forecasting errors were surprisingly similar when forecasting PBL processes. RAMS and MM5 managed to accurately capture terrain-induced

circulations and valley induced divergence and convergence at very high resolutions (Zhong and Fast 2003). A more recent study conducted by Pirovano et al. (2007) reveals that the strongest discrepancies between the models occurred within the PBL where the processes were terrain-driven. When forecasting modeled wind circulation and temperature profile, RAMS and MM5 performed similarly in agreement with observation; RAMS presented a bias towards greater wind intensity (Pirovano et al. 2007).

To the authors' knowledge, this is the first study in which MM5 and RAMS responses to perturbed SM were compared. The study assesses if the atmospheric response due to SM changes noted by Quintanar et al. (2008) are consistent with other models. This study also addressed the response between the models and their respective land-surface schemes under anomalous SM conditions.

The study is organized as follows. Chapter 2 describes the models initialization parameterizations, numerical assumptions and initial and boundary condition. This section also provides a detail description of the experimental design and the synoptic events in question. Chapter 3 presents the results of the study. Each event was individually analyzed. Chapter 3 also addressed the overall tendencies of each model. Finally, Chapter 4 provided a summary of the project and

concluding remarks.

CHAPTER 2

STUDY AREA AND METHODOLOGY

The study region was centered over western Kentucky which provided an ecological, physiographical, and climatologic transition zone, bordered by the Mississippi river to the west, the Appalachian Mountains to the east, a relatively dry Midwest region to the north, and a wetter region to the south (Quintanar et al. 2008). The models domains consisted of a single 160x120 grid-point mesh with 12 km horizontal resolution. The domain area was increased, with respect to Quintanar et al. (2008) experiments, in order to allow for better assimilation of initial boundary conditions. Furthermore, a higher horizontal resolution was selected to allow the evolution of smaller mesoscale features.

The experiments were conducted by using MM5 version 3 and RAMS. The aforementioned mesoscale models consist of three-dimensional, primitive, non-hydrostatic equations with terrain-following vertical coordinates. MM5 and RAMS also provide multiple parameterization options for turbulent mixing, advection,

TABLE 1. Summary of model specifications and parameterizations for the current study.

	RAMSv4.4	MM5
Cumulus Parameterization	Modified Kuo (Tremback et al 1994)	Kain and Fritsch (1993)
Cloud Microphysics	Walko et al. (2000)	Dudhia (1989)
Radiation	Chen and Cotton (1987)	Dudhia (1989)
Land Surface Model	LEAF2 (Walko et al. 2000)	Noah-LSM (Chen and Dudhia 2001)
Grid Structure	Arakawa C stagger	Arakawa B stagger
Projection	Rotated Polar stereography	Lambert Conformal

lateral and vertical boundary conditions, soil and vegetation, convection, and short and long wave radiation. Despite numerous similarities, each model was initialized with unique physics and convective parameterizations given their availability. Table 1 summarizes some of the various disparities among the models with respect to initialization parameterizations and grid structures.

RAMS and MM5 were initialized with a modified Kuo (Tremback et al. 1990) and Kain-Fritsch parameterization schemes (Kain and Fritsch 1993; Kain 20004), respectively. This was done due to restrictions in the model options. RAMS does not include multiple convective parameterization schemes. It has options for a

modified Kuo scheme (Tremback et al. 1990) and no parameterization. The latter is only permissible for simulations with horizontal resolution less than 4 km. Kuo (1974) has been a widely used deep cumulus parameterization scheme for large-scale and mesoscale models due to its simplicity and non-demanding computational requirements (Baik et al. 1991). The Kuo deep-cumulus convection relies on the notion that cumulus heating and moisture of large scale circulation is proportional to the temperature and water vapor mixing ratio difference between the environment and the parcel (Kuo 1974; Tremback et al. 1990; Baik et al. 1991). The resulting estimations of vertical velocities, momentum, and moisture difference can be used in order to compute vertical transport of sensible heat, horizontal momentum, and moisture among other deep cumuli quantities (Kuo 1974).

On the other hand, MM5 uses a version of the Kain-Fritsch cumulus convective parameterization (Kain and Fritsch 1993; Kain 2004) that includes shallow convection. This scheme is a mass flux parameter scheme that approximates the properties of convective clouds using the Lagrangian parcel method and vertical momentum dynamics (Kain 2004). Kain-Fritsch parameterization has proven superior to Kuo and modified-Kuo schemes for convective events such as frontal precipitation, monsoon systems, and tropical

weather (Kuo et al. 1996; Wang and Seaman 1997; Pereira et al. 1999; Yang et al. 2000; Saleeby and Cotton 2004). Yang et al (2000) suggested that Kain-Fritsch scheme offers superior skill over Kuo since it provided better estimates of the effects of convection at the mesoscale, while Kuo and modified-Kuo schemes better represent the large-scale effect of convective systems.

RAMS and MM5 were coupled with Land Ecosystem-Atmosphere Feedback model (LEAF2; Walko et al., 2000) and Noah Land Surface Model (LSM; Chen and Dudhia 2001 and reference therein) respectively, in order to account for the heat and moisture exchange between the soil, vegetation, canopy, surface water and atmosphere. The processes accounted for by the LSM models are summarized in Figure 1. The initial and boundary conditions were provided by 1°x1° NCEP Final Global Data Analysis System (FNL; http://dss.ucar.edu/datasets/ds083.2/) every 6-h. FNL dataset provides SM information (temperature and humidity) at four layers: 10 cm, 40 cm, 100 cm and 200 cm. Due to the lack of a consistent and reliable SM observation network and the limitations of remote sensing techniques, the verification of simulated SM remains challenging (Shao and Henderson-Seller 1996; Houser et al. 1998; Motovilov et al. 1999).

The MM5 LSM was initialized with four soil levels as provided by FNL

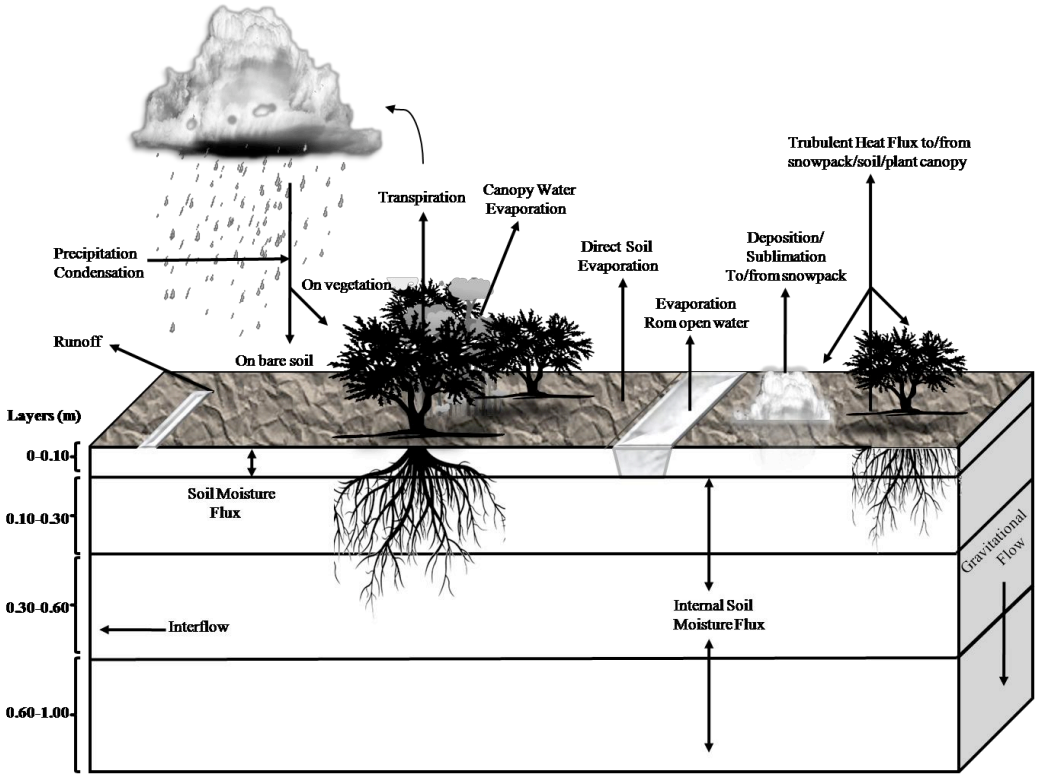

Figure 1 , Graphical representation of land surface model processes

dataset. Unlike the MM5 LSM, the LEAF2 initialization does not take into account grid-point variations of SM. The RAMS LEAF2 initializes SM homogeneously across the domain at each defined layer despite changes and variations at the sub-grid level. This representation is rather unrealistic since it does not account for topographic disparities, soil type, and variations of land uses which have been

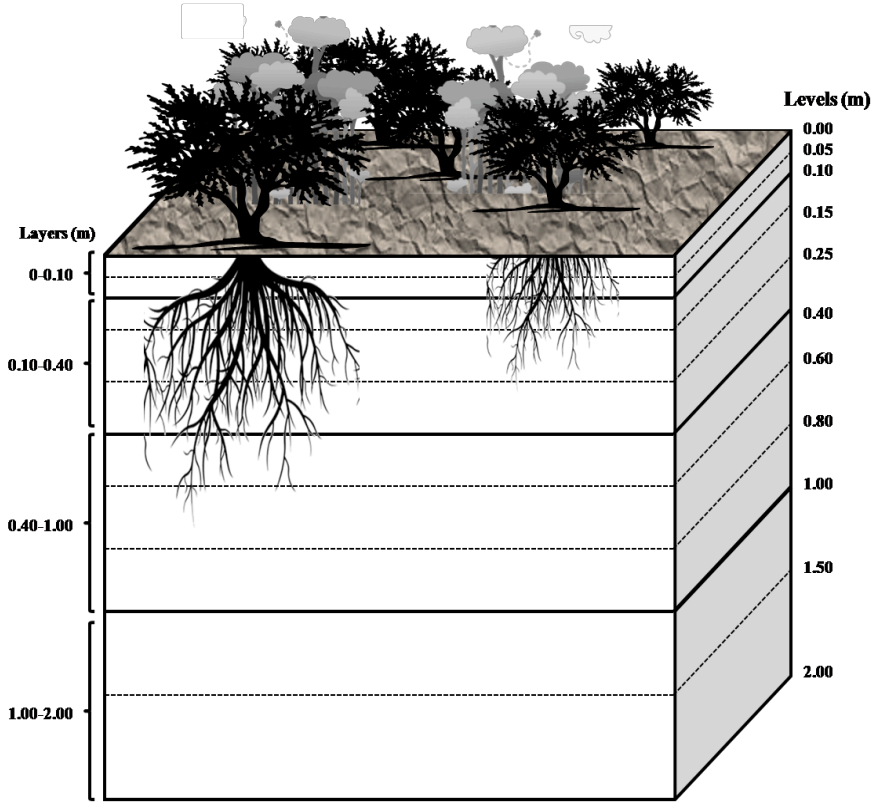

Figure 2. Soil layer as defined on RAMS (left) and FNL layers (right)

shown to affect SM (Ookouchi et al. 1984; Mahmood and Hubbard 2003). Modifications were needed in order to successfully initialize LEAF2 from FNL data. The LEAF2 initialization procedure (leaf2_init.f90) was altered in order to input FNL SM data. Four layers were defined: 0.0-0.1, 0.1-.4, 0.4-1.0, and 1.0-2.0 m. The aforementioned was accomplished by establishing 11 levels, as seen in Figure 2. SM

was initialized at the beginning of each simulation and allowed to vary given the development and distribution of precipitation within the model. The proper initialization of SM in RAMS was assessed by comparing the initial values with respect to FNL data (not shown). Additional modifications were also required in order to verify the successful initialization of SM in LEAF2. RAMS post processing tool, RAMS/HYPACT Evaluation and Visualization Utilities (REVU, Tremback et al. 2002) was altered in order to allow for the output of SM at all available levels. Some of the modifications performed to LEAF2 were summarized in Appendix 1.

SM was homogeneously and uniformly perturbed throughout the models' domain in order to preserve horizontal and vertical gradients of moisture. The perturbations of SM were consistent with Quintanar et al. (2008) experimental design. SM was increased (wet) and decreased (dry) by 0.05, 0.10, and 0.15 m^3m^{-3} for all the time periods examined. Experiments in which SM was increased are referred to as WP05, WP10, and WP15, respectively herein. On the other hand, dry experiments are referred to as DP05, DP10, and DP15 respectively. The simulations were integrated over a 24 hour period initialized at 12 UTC for each study period. The set of experiments was conducted with both mesoscale models.

Unlike previous studies in which SM was simply multiply by a factor larger or

smaller than unity in order to introduce horizontal and vertical moisture gradients, fixed values were added and subtracted from the initial values of SM in order to avoid model induced mesoscale circulations (Oockuchi et al. 1984; Quintanar et al. 2008). Given the initial high SM conditions over the southeastern region during June of 2006, no lower boundary of soil wetness was required for the study. On the other hand, upper boundaries of SM were enforced for the wet experiments. As indicated before, the study region consisted of various soil types including sand, loam, and clay. Thus, the upper boundary was defined by the average of each soil type's field capacity which is 0.42 m^3m^{-3}. The perturbations were sufficient to allow the soil to become under and super saturated which was expected to have significantly different effect on PBL depth and evolution (Leeper et al. 2009; Mahmood et. al. 2009). Wetter soils have been shown to be conducive to producing shallower PBL, while dryer environment have been shown to enhance turbulent mixing thus PBL depth (Quintanar et al. 2008).

The simulations consisted of 31 levels of vertical resolution. Experiments were conducted in order to assess the models' dependency on vertical resolution. The experiment with 31 vertical levels did not differ significantly from those with higher number of vertical levels; this vertical resolution produced precipitation

quantities similar to observed values on MM5. Simulated precipitation was verified with the North American Regional Reanalysis (NARR; Messinger et al. 2004, Mitchell et al. 2004). NARR data was selected for verification purposes since, unlike other global model reanalyzes, orographically-corrected precipitation is assimilated into the dataset providing better estimates of hydrologic variables such as SM and land surface fluxes (Luo et al. 2005).

Synoptic Events

Three synoptic events were examined during late spring and early summer of 2006: 11 June, 17 June and 22 June. The events were typical given the seasonal variations of the region and presented various degrees of synoptic forcing ranging from weak, moderate, to strong. The 11 June event was characterized by a stationary front extending through Nebraska, Missouri, Western Kentucky, Tennessee, and North Carolina on 11 June at 0012 UTC. Throughout the simulation period, this frontal boundary remained stationary until 12 June at 0006 UTC in which a low pressure system developed over central Kentucky. The low pressure system had a cold front extending westward into Missouri, and Nebraska (not shown). The system progressed eastward, located over Virginia on 12 June at 0009

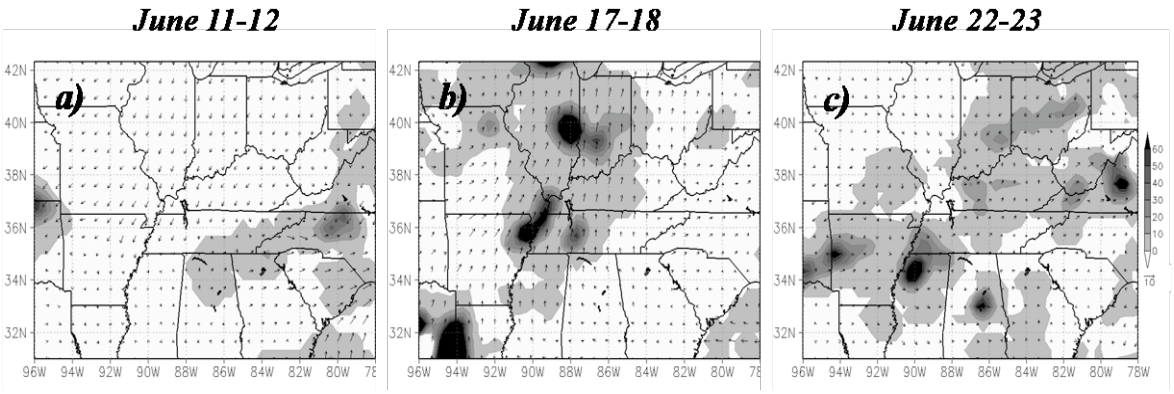

Figure 3. NARR precipitation (shaded according to scale, 10 mm) accumulation for a 24 h period centered at 0000 UTC for each event.

UTC. The cold front had been displaced southward. Through the Midwest and Kentucky, winds were from the north and temperatures were in a decreasing mode. The system produced significant precipitation with some regions experiencing up to 30 mm. The 11-12 June event was a moderate synoptically driven event as defined by Quintanar et al. (2008).

A six day drying period preceded the event of 17 June due to the presence of a high pressure system over Eastern United State. The 17-18 June event was enhanced by strong warm moist air advection from the Gulf of Mexico. The low pressure system was located over northern Michigan at 0000 UTC on 18 June. The system was accompanied by a cold frontal boundary extending from Wisconsin

through Oklahoma. Strong south winds with speeds of up to 8 m s^{-1} helped advect warm moist air into the southeastern region. As a result of the interaction with the cold front, precipitation developed along the frontal boundary with convective clusters found as far as Kentucky. This event produced significant amounts of precipitation over Western Kentucky exceeding 40 mm. This event was identified as highly enhanced by synoptic features and circulation.

On the other hand, the last event examined, on 21 June, was weakly influenced by the synoptic setting. A stationary boundary extended from Colorado to Iowa, where the surface low was located at 0012 UTC 21 June. To the east of this feature, a warm front was present extending through Ohio. By 0012 UTC 22 June, a cold front had developed in association with an occluded low over the Canadian province of Quebec. The cold frontal boundary extended through the Great Lakes. The precipitation event over Kentucky was enhanced by the presence of warm air advection from the Gulf of Mexico. Wind speeds during this event ranged from calm to 5 m s^{-1}. The event produced significant precipitation over the region of study with recorded amounts of 25 mm. Despite apparent similarities among the events, they presented varying synoptic forcing and convective activities which allowed us to examine the influence of SM on various synoptically driven convective events.

CHAPTER 3

RESULTS AND DISCUSSION

Figure 4 shows 24-h accumulated precipitation centered at 0000 UTC for all CTRL simulations. While both models managed to capture the overall synoptic circulation for all three events, the distribution and accumulation of precipitation varied with respect to NARR data (see Figure 3). On 11-12 June, MM5 produced significantly more precipitation than NARR. MM5 positioned precipitation maxima–exceeding 40 mm—extending from southern Indiana into northern Kentucky (see Figure 4a). This CTRL simulation produced 21 mm more than observed. On the other hand, RAMS produced a large area of light precipitation ranging between 0.1 and 10 mm over most of the domain. It produced less precipitation than MM5 with 24-h accumulations not exceeding 20 mm. Compared to NARR, based on the visual inspection, RAMS produced the most satisfactory simulation for the 11-12 June event. Both models generally resolved the strong warm and cold air advection over the southwestern and northwestern corner of the domain, respectively.

For June 17-18 event, MM5 resolved precipitation amounts ranging from 20

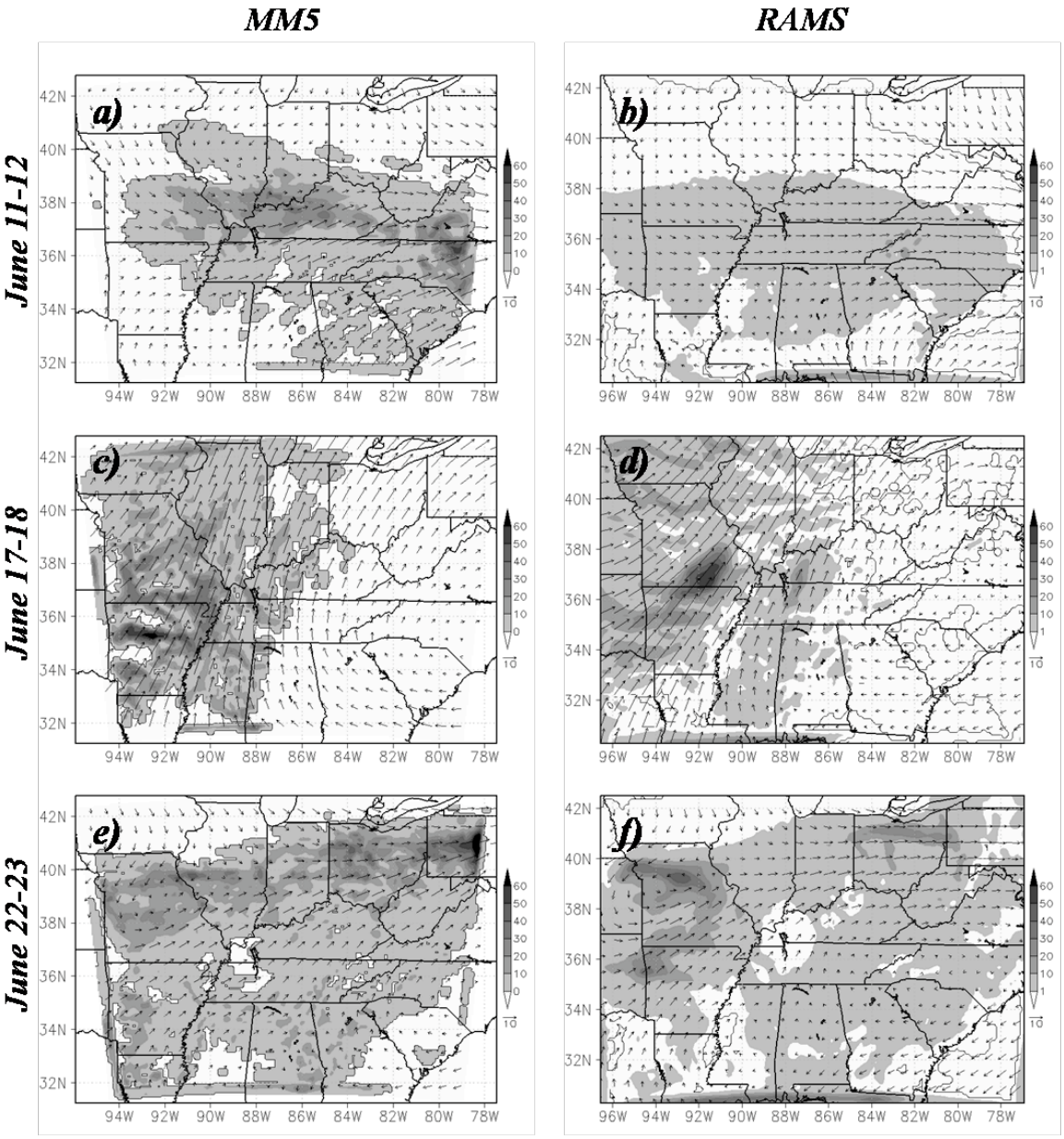

Figure 4. MM5 and RAMS CTRL 24-h precipitation accumulation (shaded according to scale, 10 mm) and horizontal wind velocities (vector, 10 ms^{-1}) centered at 0000 UTC for each event.

to 40 mm over most of Alabama, Missouri, Illinois and western Kentucky. A precipitation maximum exceeding 60 mm was located over northern Arkansas. MM5 positioned this maximum slightly to the east of the observed precipitation core (see Figure 3b). Furthermore, RAMS produced multiple precipitation maxima over the Missouri-Arkansas border. RAMS CTRL simulation positioned a precipitation maximum over southern Arkansas with accumulation quantities exceeding 50 mm. For this event, both models fail to accurately position the precipitation core over the Oklahoma-Arkansas border, as seen in Figure 3b, and to accurately resolve the overall accumulation for the event. On the other hand, both models managed to capture the strong warm-air advection present during 17-18 June.

On 21-22 June, MM5 simulated light precipitation, ranging from 0 to 10 mm, over most of the domain. It resolved multiple precipitation maxima extending from central Illinois to northern Ohio and Pennsylvania. This simulation produced significantly more precipitation than NARR with maxima exceeding 60 mm accumulations. On the other hand, NARR reported an accumulation maximum less than 20 mm for June 21-22. Nevertheless, RAMS simulated a precipitation maximum over northern Missouri with accumulations exceeding 40 mm. RAMS also resolved a small accumulation over northwestern Arkansas and northern Ohio not observed on

NARR. Neither mesoscale model was able to accurately simulate the precipitation accumulation and distribution. On the other hand, RAMS and MM5 were able to resolve the cyclonic circulation over central Missouri, feature which characterized this event.

Overall the models compared relatively well with respect to observations although they are not able to accurately resolve precipitation accumulations. RAMS and MM5 produced vast regions of light precipitation through the entire domain for all simulations. Both models managed to resolve the strong warm air advection which characterized these events. MM5 and RAMS also manage to resolve the shallow cyclonic circulations associated with the 11-12 and 21-22 June events.

Sensitivity of MM5 and RAMS to SM Modifications

Six simulations were conducted for each study period in which θ_e, vertical velocities, latent and sensible heat fluxes, and precipitation were analyzed. All the aforementioned variables were also examined by Quintanar et al. (2008) since they showed to be good indicative of precipitation development. Stability is analyzed using θ_e as a proxy for moist static energy (Pielke 2001; Quintanar el al. 2008). Quintanar et al. (2008) demonstrated that θ_e was more sensitive to SM variations

than the lifted condensation level and the convective available potential energy. In addition, sensible and latent heat fluxes were also explored by Quintanar et al. (2008) by using Bowen ratio. Large latent heat fluxes coupled with horizontal gradients of SM and a lifting mechanism can generate deep cumulus convection (Belts et al. 1996; Pielke 2001, Quintanar et al. 2008). Finally, vertical velocities were examined as a lifting mechanism for deep convection and a good indicative of precipitation rate (Quintanar et al. 2008).

11-12 June 2006

Precipitation and horizontal wind field

Figure 5 summarizes the precipitation differences between each dry experiments and CTRL simulations. MM5 presented little variation among dry experiments. As expected, they (Fig 5. a, c, e) produced slightly less precipitation than CTRL for decreasing SM, displacing the precipitation maxima east of the Appalachians. Sharp gradients of precipitation can be observed over North Carolina for all three experiments. On the other hand, small accumulation maxima can be observed over western Kentucky for MM5 DP05 and DP10 in which the simulation produced slightly more precipitation than CTRL. On the other hand, MM5 wet

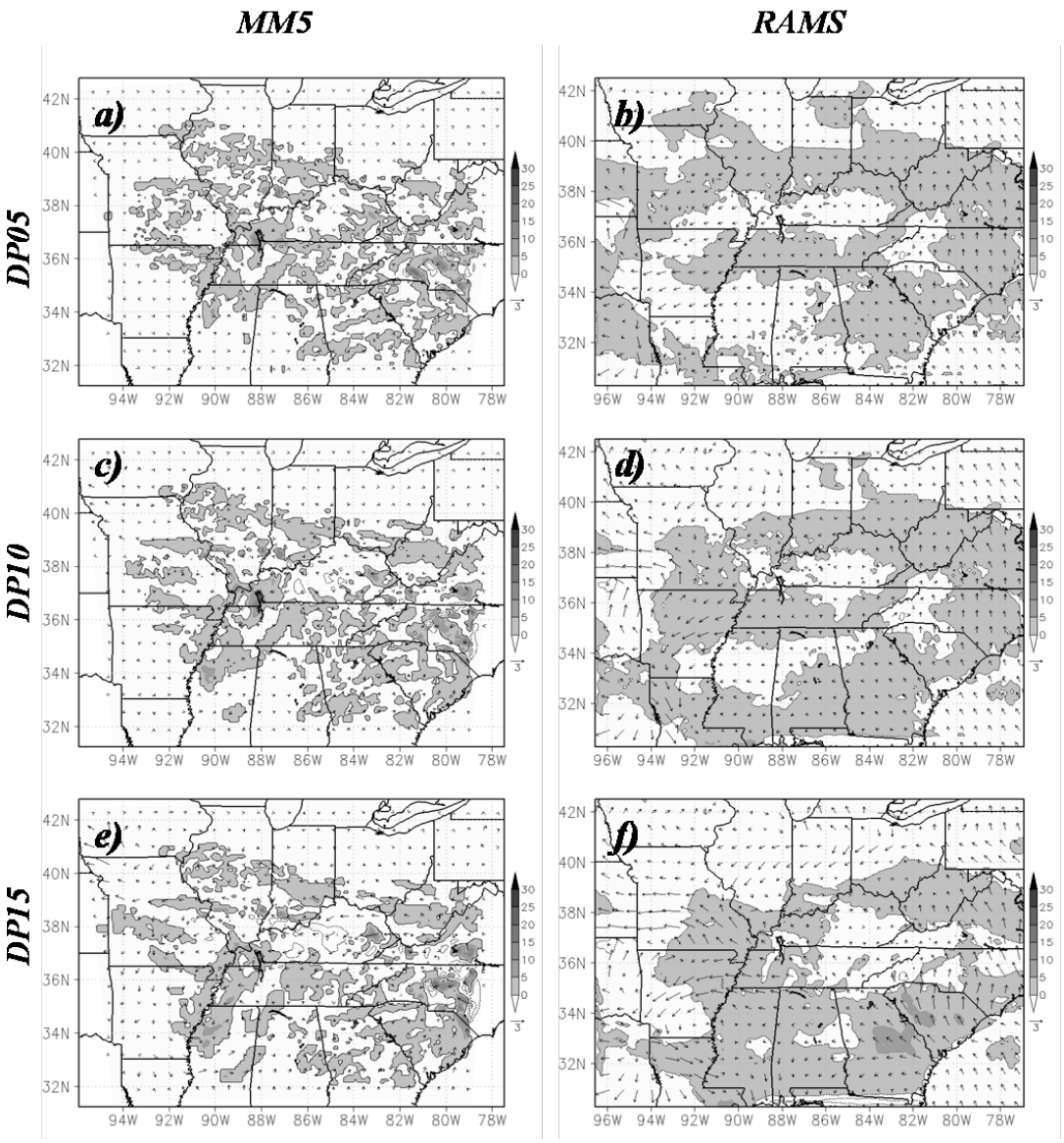

Figure 5. MM5 and RAMS dry experiment minus CTRL precipitation (positive values shaded according to scale, negative values contoured, 5 mm) and horizontal wind velocities (vector, 3 ms^{-1}) for 11-12 June

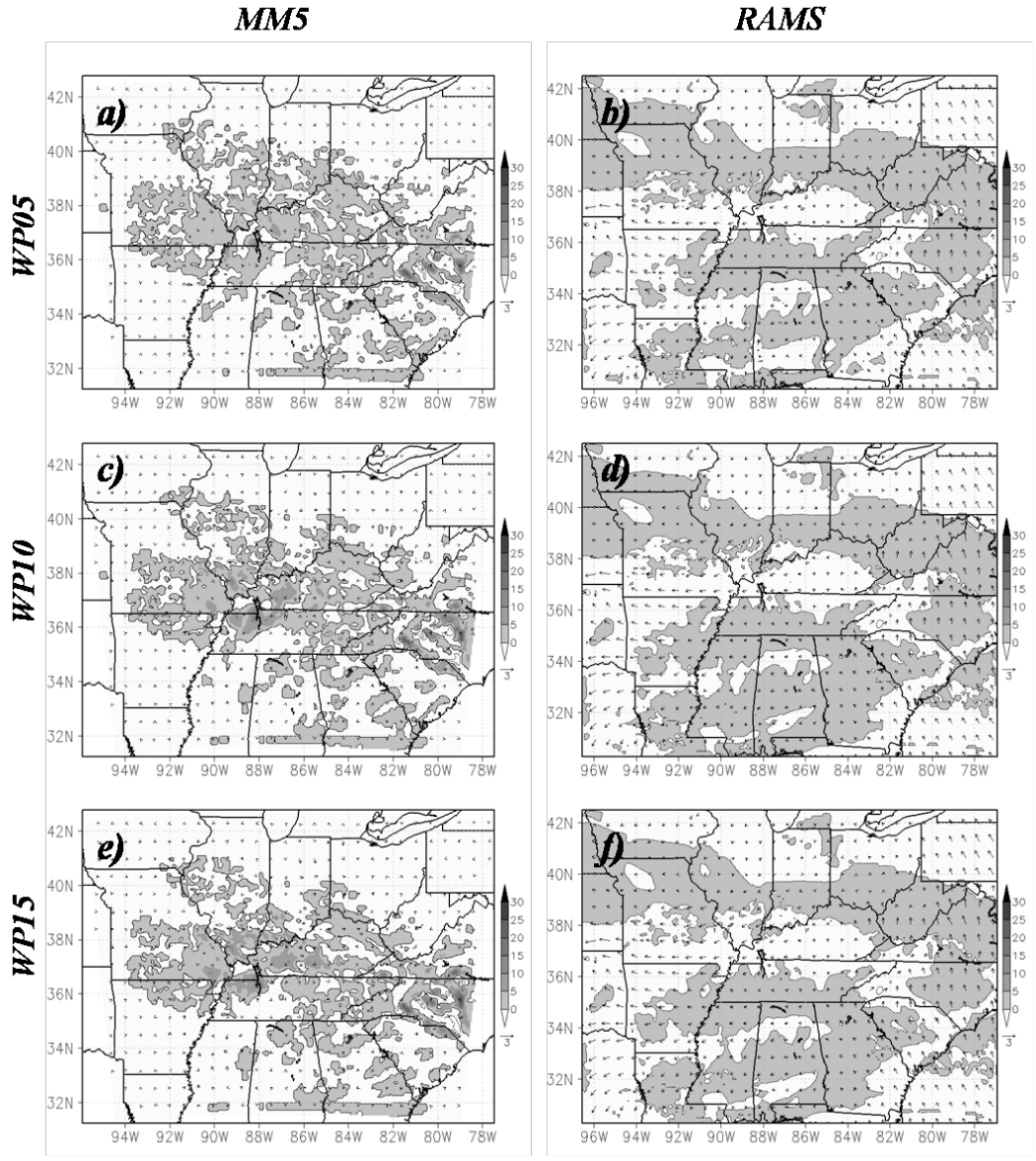

Figure 6. MM5 and RAMS wet experiment minus CTRL precipitation (positive values shaded according to scale, negative values contoured, 5 mm) and horizontal wind velocities (vectors, 3 ms^{-1}) for 11-12 June.

experiments—as seen in Figure 6—presented more variations among each other. Positive perturbations of soil moisture resulted on increased precipitations of all three wet experiments. The most pronounced variations of precipitation accumulations were located over North Carolina. The higher gradients of accumulation can be attributed to the displacement of the precipitation within this region. Higher precipitation accumulations were recorded over western Kentucky, where a precipitation differences between WP10 and WP15 and CTRL exceeded 15 mm.

RAMS dry experiments for 11-12 June, on the other hand, presented little variation among each other with respect to precipitation. DP05 and DP10 presented variations of less than 5 mm with respect to CTRL. Only DP15 produced over 10 mm of precipitation more than CTRL over central Georgia and eastern South Carolina. For a small region over eastern North Carolina, all three experiments produced less precipitation than CTRL. Positive perturbations of SM were less conducive of precipitation variations. WP05, WP10, and WP15 produced accumulations less than 5 mm from CTRL.

Perturbed SM did not produced significant variation for MM5 simulations wind fields. Both dry and wet experiments presented little to no variations of wind

speeds with respect to CTRL. Only DP15 presented wind speed differences over North Carolina where the precipitation maxima between the experiment and CTRL were displaced. On the other hand, perturbations of SM induced circulations for RAMS dry and wet experiments. Decreases in SM were conducive of increased wind speed differences between the experiments and CTRL. Positive perturbations of SM were not conducive of strong horizontal wind speed differences between the experiments and CTRL.

Equivalent Potential Temperature

θ_e was also examined with respect to CTRL simulations. Figure 7 presented the differences between averaged θ_e for dry simulations and CTRL over a 12-h period centered at 0000 UTC on 12 June. θ_e was shown as a vertical cross-section at 37°W latitude extending from 94°W to 78°W longitude. 37°W latitude was selected since, as seen in Figure 3, it encompassed the regions of strongest precipitation to the west of the domain, and little to no precipitation to the east for all three synoptic events in question. The cross-sections were examined through 900 to 200 hPa. The described properties were selected for all cross-sections examined.

MM5 dry experiments did not produced significant variations from CTRL

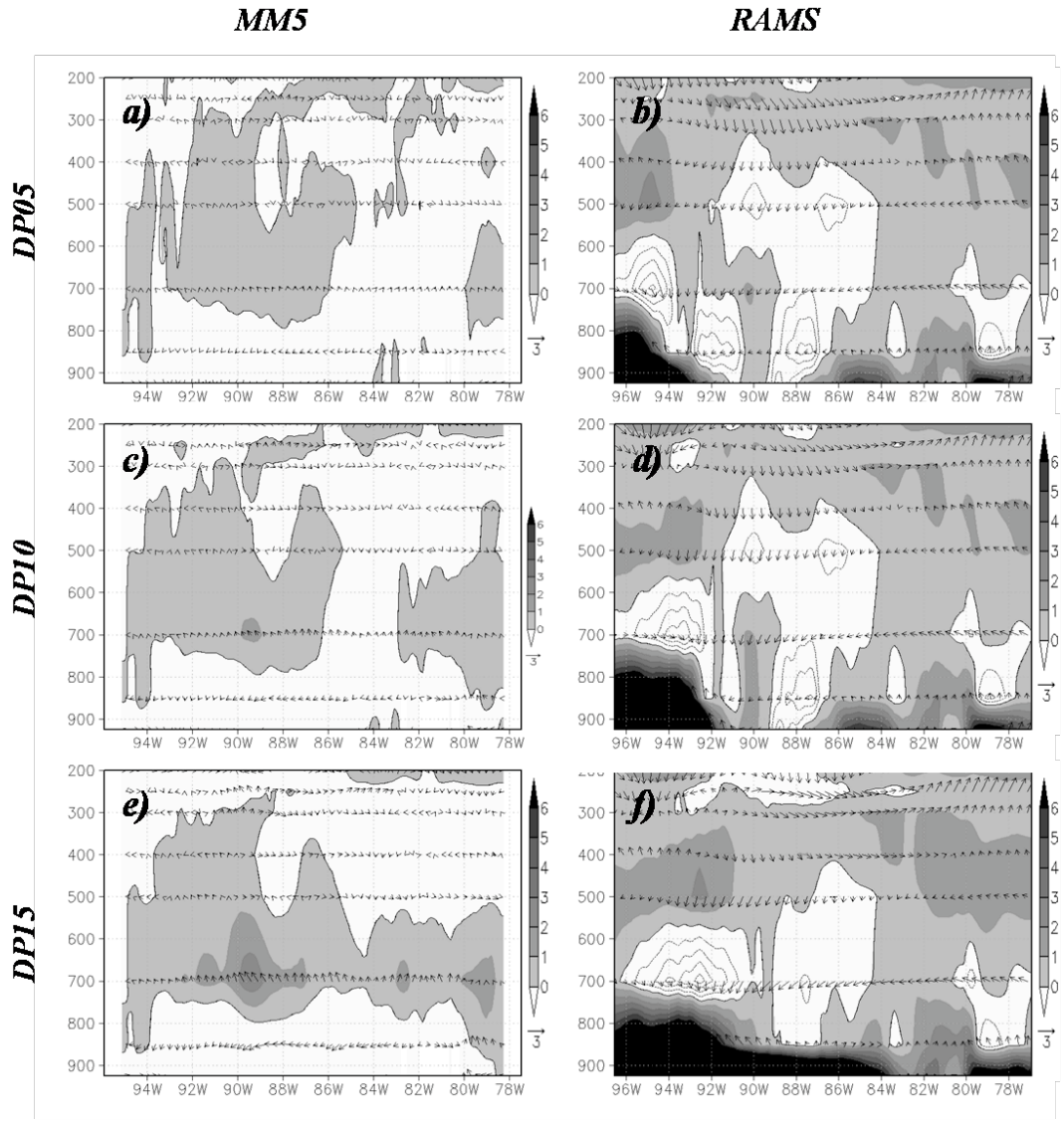

Figure 7. MM5 and RAMS dry experiment minus CTRL cross-sections of 12-h averaged equivalent potential temperature (positive values shaded according to scale, negative values contoured, K) and horizontal wind velocities (3 ms^{-1}) for 94°W to 78°W longitude and 37°W latitude centered at 0000 UTC on 12 June

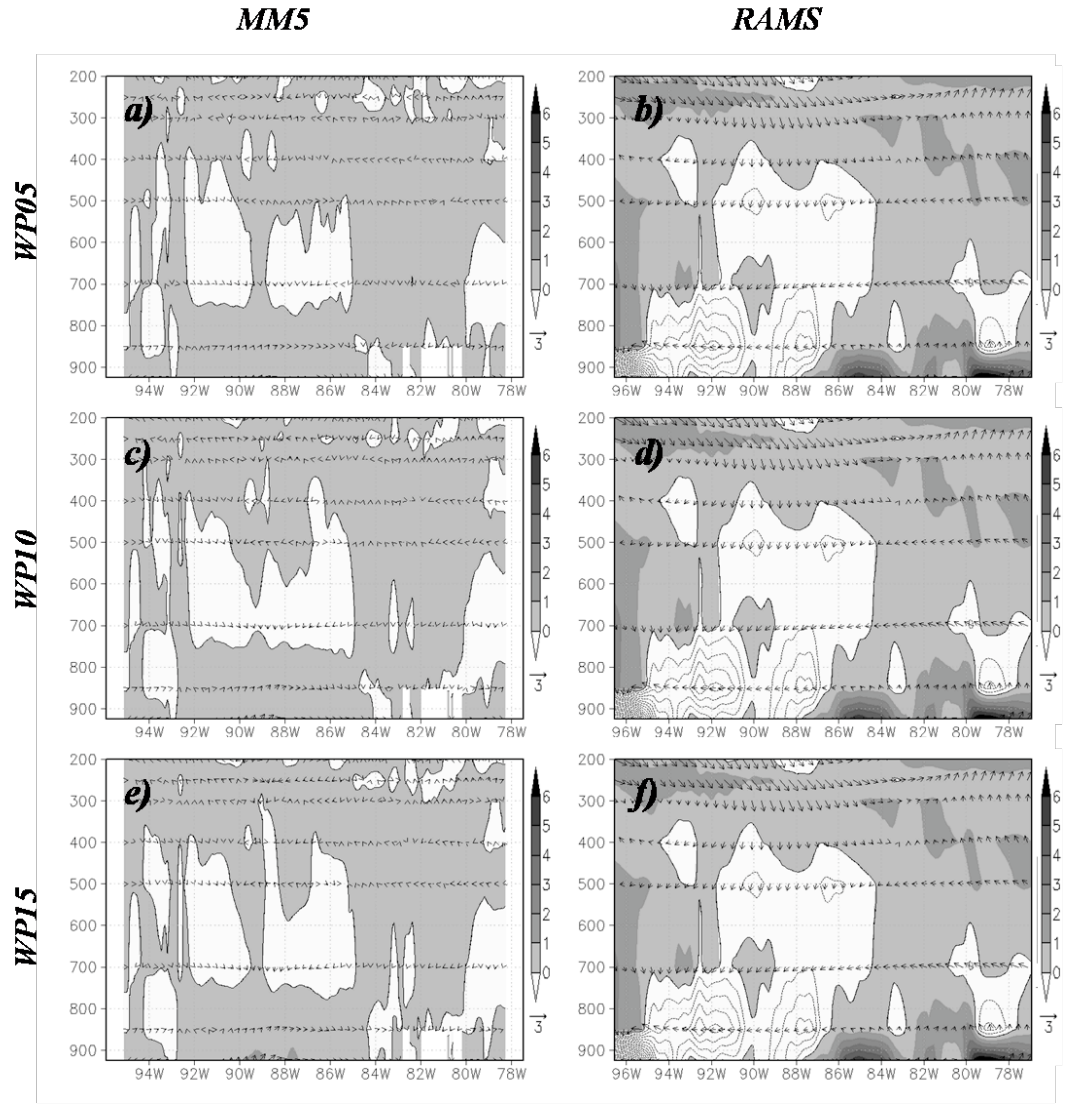

Figure 8. MM5 and RAMS wet experiment minus CTRL cross-sections of 12-h averaged equivalent potential temperature (positive values shaded according to scale, negative values contoured, K) and horizontal wind velocities (3 ms^{-1}) for 94°W to 78°W longitude and 37°W latitude centered at 0000 UTC on 12 June

runs at the lower 150 hPa. Differences between average θ_e for DP05 and DP10 and CTRL were less than 1 and 2 K respectively. DP15, on the other hand, simulated θ_e values up to 4 K greater than CTRL. The maximum difference between DP15 and CTRL was located around 700 hPa. This height represented the upper boundary of the PBL. On the other hand, wet experiments presented little to no variation with respect to control. All three experiments, compared to CTRL, simulated θ_e less than 1 K for most of the domain. WP10 and WP15 produced higher θ_e less CTRL between 90°W and 87°W longitude at 900 hPa where the precipitation maximum was located.

RAMS dry simulations presented significant θ_e differences with respect to CTRL. DP05, DP10 and DP15 experiments simulated greater θ_e values exceeding 6 K over the western region of the domain, where the precipitation maxima develops. The 900 hPa positive maxima were located between 94°W and 92°W longitude for all three experiments. A strong gradient can be observed between the maxima and 700 hPa. On the contrary, wet experiments produced significantly lower θ_e than CTRL to the west of the domain. Multiple positive surface θ_e maxima could be observed in Figure 8 between 86°W and 78°W longitude with value exceeding 6 K between WP05, WP10, WP15 and CTRL.

3-D Vertical Wind

3-D wind velocities were also examined as a cross-section located at 37°N latitude. The vertical cross-section extended horizontally from 94°W to 78°W longitude and 900 to 200 hPa vertically. Vertical velocities was averaged over a period of 12-h centered at 0000 UTC 12 June. Figure 9 presented dry simulations minus CTRL values of the vertical and horizontal wind fields with respect to CTRL. MM5 DP05, DP10, and DP15 simulations presented significant variations of vertical wind velocities at 88°W longitude. DP05 produced the strongest vertical motions over Kentucky with respect to CTRL exceeding 12 cm s^{-1} at the upper levels. The vertical wind maximum extended from the surface to 250 hPa. This feature corresponded with the region in which MM5 produced the highest precipitation accumulation. Positive perturbations of SM also produced regions of increased vertical velocities with respect to CTRL. Although the increased of vertical velocities due to increased SM was not as pronounced as for dry experiments, these feature was observed for all wet experiments. Vertical wind maxima between the experiment and CTRL ranged from 2 to 8 cm s^{-1} and were located at 88°W longitude were the precipitation maxima on the cross-section was located.

On the other hand, RAMS DP05, DP10, and DP15 resolved a vertical velocity

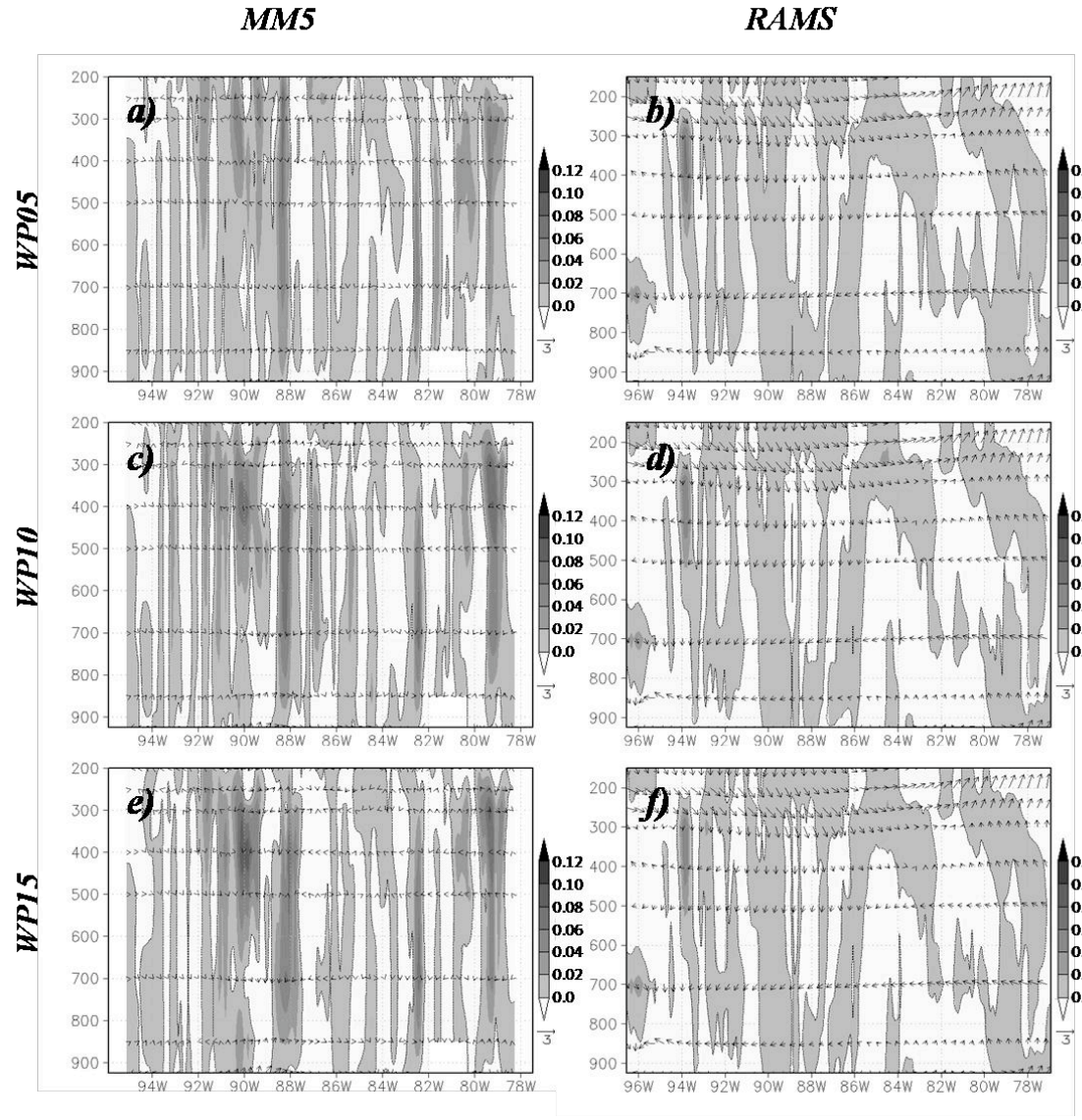

Figure 9. MM5 and RAMS wet experiment minus CTRL cross-sections of vertical wind profile (positive values shaded according to scale, negative values contoured, ms^{-1}) and horizontal wind velocities (vector, 3 ms^{-1}) for 94°W to 78°W longitude and 37°W latitude centered at 0000 UTC on 22 June

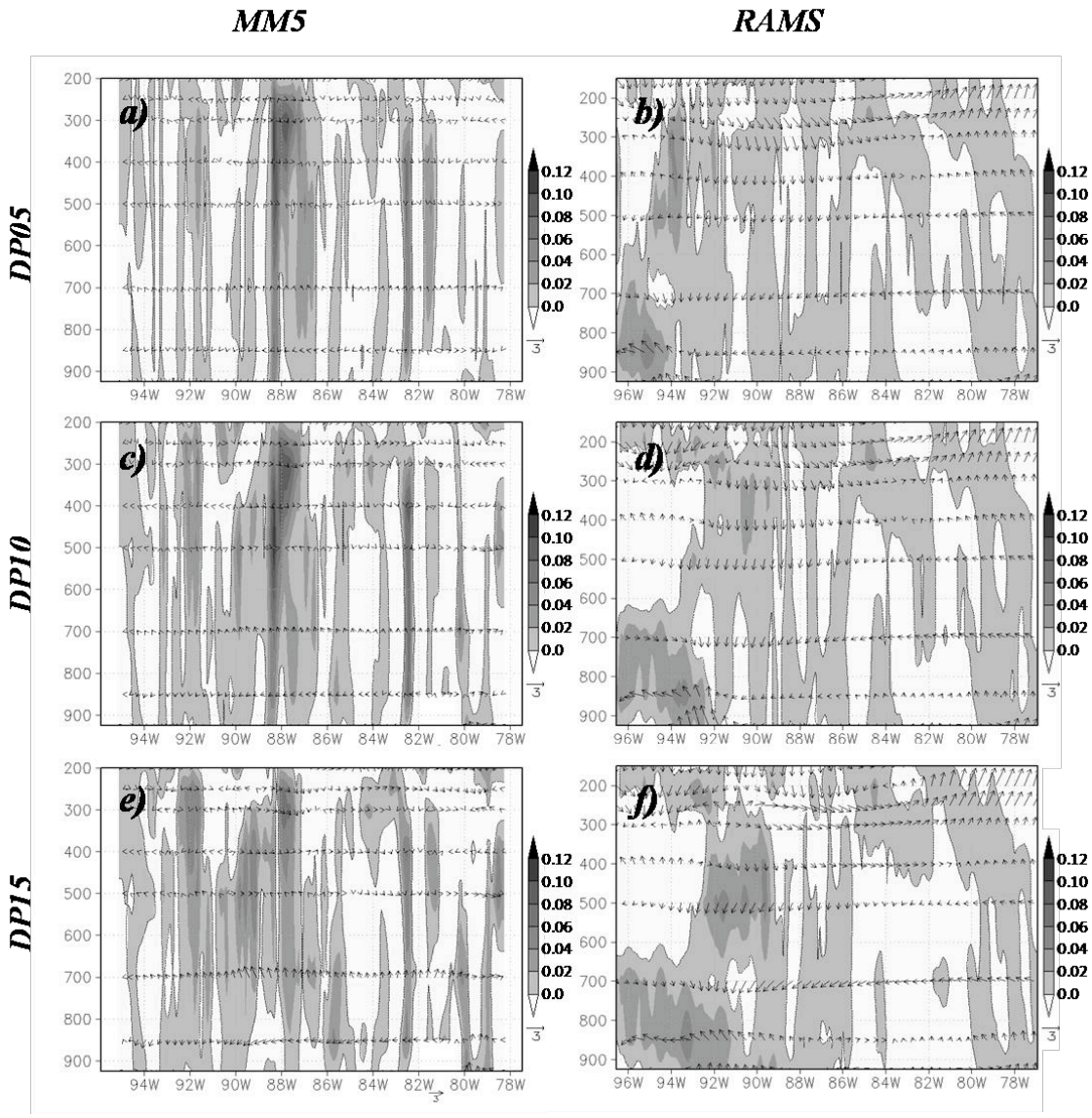

Figure 10. MM5 and RAMS dry experiment minus CTRL cross-sections of vertical wind profile (positive values shaded according to scale, negative values contoured, 0.02 ms^{-1}) and horizontal wind velocities (3 ms^{-1}) for 94°W to 78°W longitude and 37°W latitude centered at 0000 UTC on 12 June.

maximum over the western portion of the domain with respect to CTRL. The maxima were located at 95°, 94°, and 93° W longitude for DP05, DP10 and DP15 respectively. The enhancement of the vertical wind profile can also be observed through the horizontal wind in which positive circulation can be observed around the vertical wind maxima for all three events (see Figure 10 b, d, f). As seen in MM5 wet experiments, RAMS WP05, WP10, and WP 15 produced regions where vertical wind velocities were enhanced by increases in SM. A 10 cm s^{-1} maximum was observed at 94°W longitude and extending from 500 to 300 hPa.

Latent Heat Flux

Figure 11 summarized 12-h averaged latent heat fluxes minus CTRL simulations centered at 0000 UTC on 12 June for all dry experiments. Decreases in soil moisture were conducive of decreased latent heat fluxes for MM5 dry simulations. Figure 11 showed that negative perturbation of SM of 0.05 m^3m^{-3} did not have a significant effect on the surface latent heat fluxes, revealing regions in which CTRL produced fluxes of less than 40 Wm^{-2} over North Carolina. On the other hand, decreases of SM of 0.10 and 0.15 m^3m^{-3} produced regions in which CTRL simulated up to 120 Wm^{-2} more than the experiments. On the other hand, increases in SM resulted in increased latent heat fluxes along the Mississippi, South Carolina,

and Georgia. Figure 12 (a, c, e) revealed that with increasing SM perturbation, most of the incoming solar radiation flux gets partitioned into latent heat flux. Both WP10 and WP15 presented regions in which the experiments simulated more than 120 Wm^{-2} over the Mississippi Valley.

RAMS dry simulations of latent heat fluxes produced large regions over the western portion of the domain in which CTRL simulated over 120 Wm^{-2} greater than each experiments. On the other hand, little variations can be observed between WP05, WP10, and WP15. All wet experiments simulated small region over the eastern Oklahoma and Kansas border. In this region, WP05, WP10, and WP15 simulated latent heat fluxes greater than 120 Wm^{-2} with respect to CTRL. The three experiments revealed a southeastward of the aforementioned maxima in which CTRL produced latent heat fluxes greater than 120 Wm^{-2}. This suggests that RAMS wet experiments displaced the latent heat flux maxima northwestward as SM was increased

Sensible heat flux

Sensible heat fluxes were also examined with respect to CTRL runs. Figure 13 showed the difference between dry experiments and CTRL simulations. For MM5 dry simulations, decreases in SM resulted in increased sensible heat fluxes.

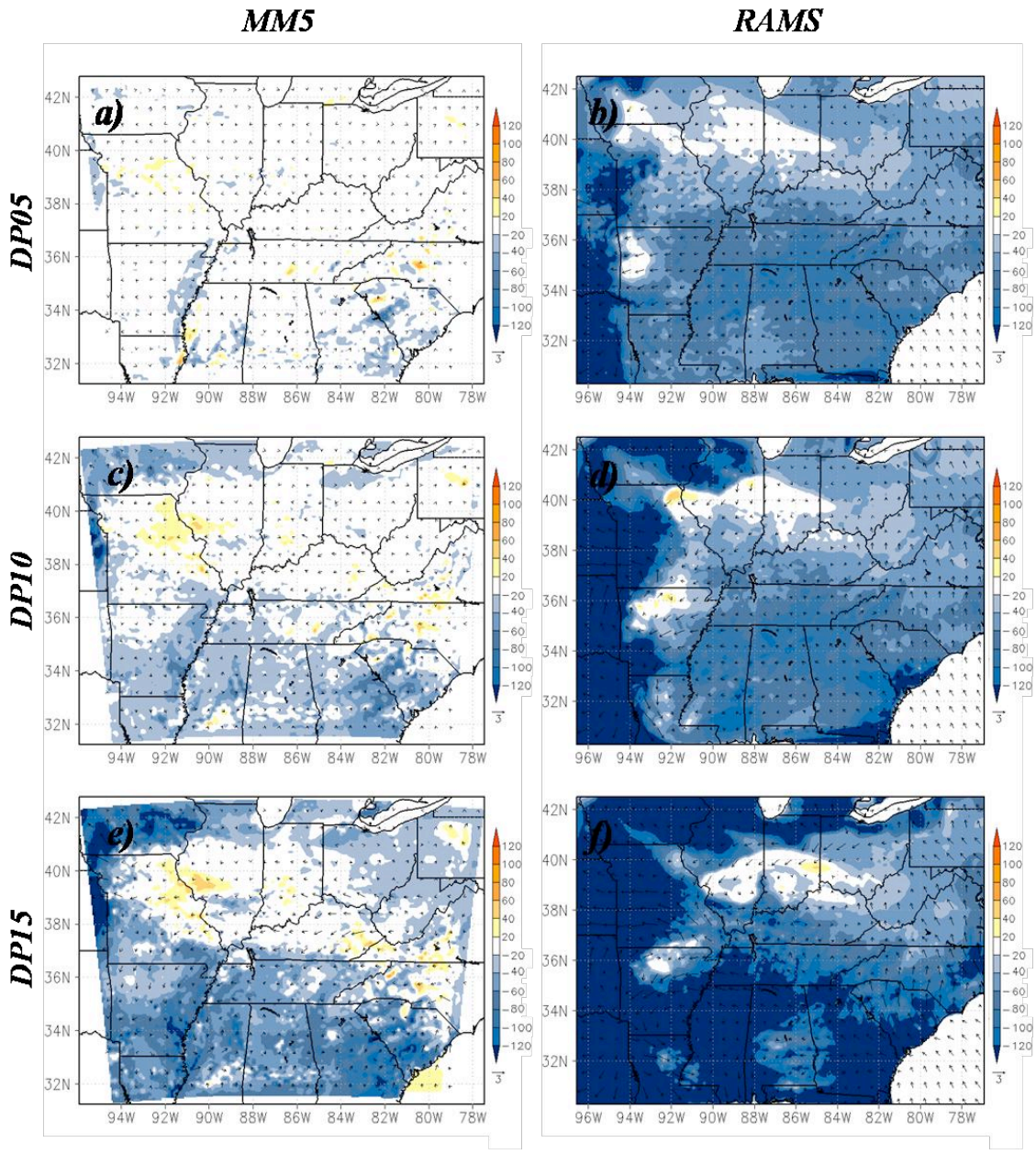

Figure 11. MM5 and RAMS dry experiments minus CTRL of 12-h averaged latent heat fluxes (positive values shaded according to scale, negative values contoured, 40 m) and horizontal wind velocities (vector, 3 ms^{-1}) centered at 0000 UTC on 12 June.

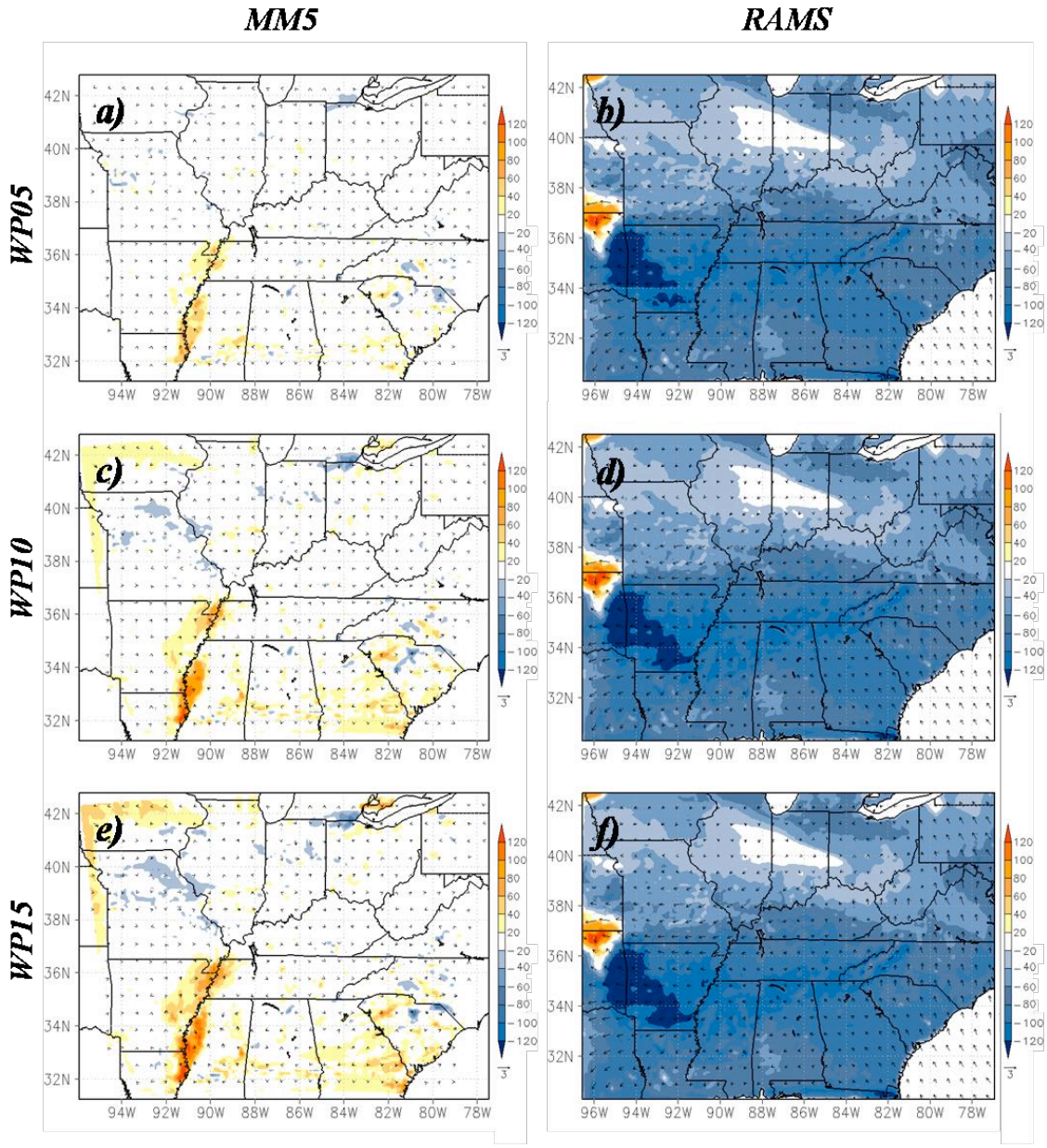

Figure 12. MM5 and RAMS wet experiment minus CTRL of 12-h averaged latent heat fluxes (positive values shaded according to scale, negative values contoured, 40 m) and horizontal wind velocities (vector, 3 ms^{-1}) centered at 0000 UTC on 12 June.

DP05 did not produced a significant increased in sensible heat flux with respect to CTRL, simulating small regions in which sensible heat flux exceeded 40 Wm^{-2}. As SM was further decreased, the differences between the DP10 and DP15 were maximized with sensible heat maxima exceeding 120 Wm^{-2} for both experiments. Increases of SM had little impact on sensible heat fluxes for WP05, WP10 and WP15 (see Figure 14 a, c, e). CTRL produced up to 40 Wm^{-2} more than all the wet experiments.

RAMS dry experiments were more sensitive to increases in SM than MM5's simulations. RAMS dry experiments simulated increased sensible heat fluxes over the western section of the domain with values exceeding 120 Wm^{-2} versus CTRL. On the other hand, for all three dry simulations vast regions developed in which decreased SM resulted in decreased sensible heat flux with respect to CTRL. RAMS WP05, WP10, and WP15 developed a sensible heat flux minima with respect to CTRL over the eastern Oklahoma and Kansas border with values exceeding 120 Wm^{-2} compared to CTRL. As expected for wet experiments, CTRL produced larger values of sensible heat flux than the simulations.

17-18 June 2006

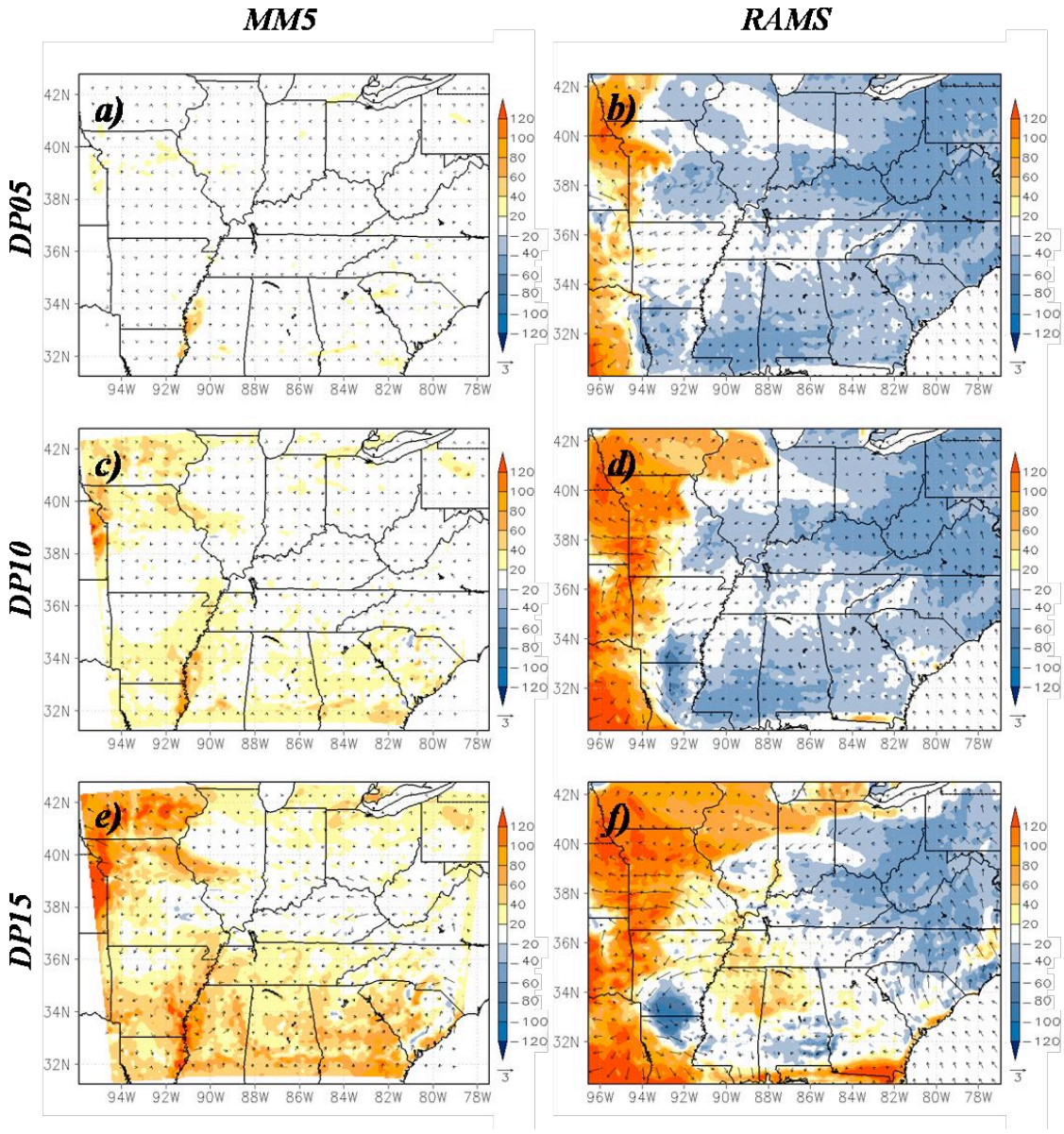

Figure 13. MM5 and RAMS dry experiment minus CTRL of 12-h averaged sensible heat fluxes (positive values shaded according to scale, negative values contoured, 40 m) and horizontal wind velocities (vector, 3 ms^{-1}) centered at 0000 UTC on 12 June.

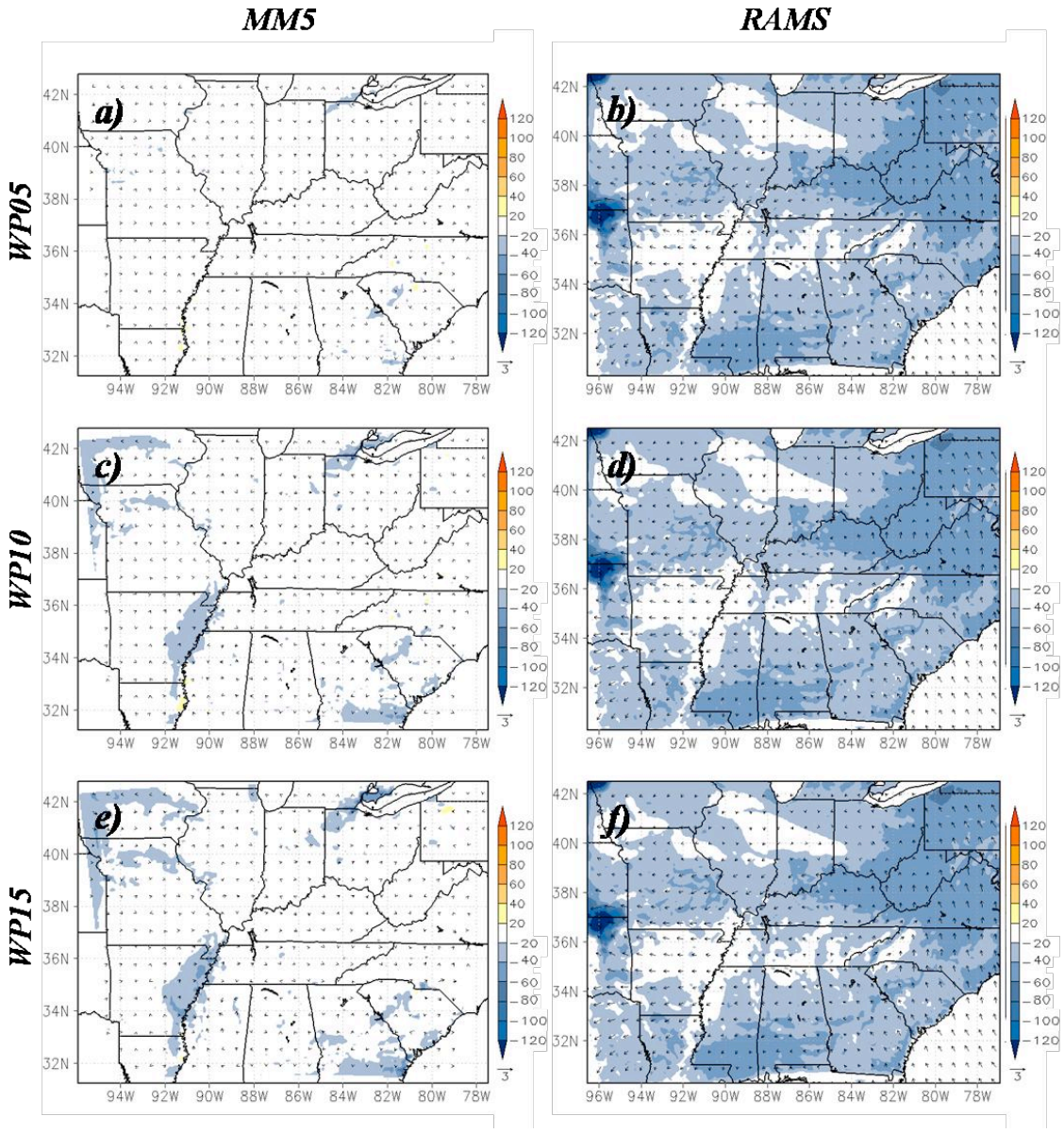

Figure 14. MM5 and RAMS wet experiment minus CTRL of 12-h averaged sensible heat fluxes (positive values shaded according to scale, negative values contoured, 40 m) and horizontal wind velocities (vector, 3 ms^{-1}) centered at 0000 UTC on 12 June.

Precipitation and horizontal wind field

MM5 dry experiments are summarized on Figure 15 (a, c, e). DP05, DP10, and DP15 displaced the location of precipitation maxima with respect to CTRL simulations. Accumulation differences between the experiments and CTRL exceed 15 mm at some locations. Overall, decreases of SM resulted in the displacement of precipitation maxima over the western sector of the domain. Positive perturbation of SM in MM5 also alters the distribution of precipitation, producing strong accumulation gradients especially for WP15, as seen in Figure 16e. This experiment also presented precipitation disparities greater than 30 mm over central Arkansas and southeastern Missouri.

While MM5 resolves moderate changes of precipitation distribution for this event, RAMS shifted the main precipitation cluster southeastward. Although precipitation was expected to behave differently under perturbed conditions, both wet and dry experiments displaced location of precipitation maxima observed in the CTRL and observational data. During this event, RAMS wet and dry simulations displaced the main precipitation core from central Missouri into northern Arkansas. Despite the similarities among the simulations with regards to the displacement of precipitation, overall, dry experiments produced less precipitation than wet. DP15

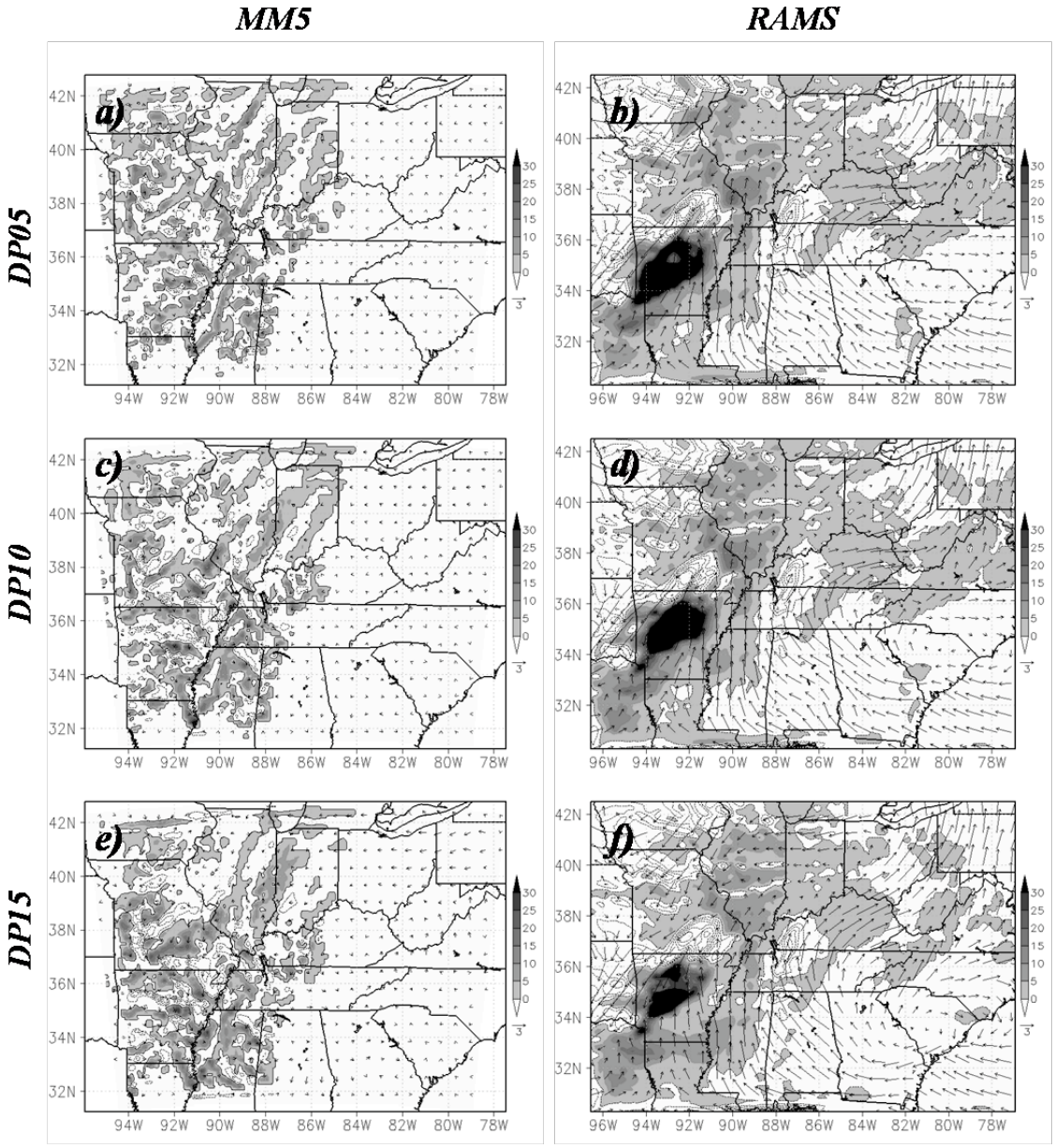

Figure 15. MM5 and RAMS dry experiment minus CTRL precipitation (positive values shaded according to scale, negative values contoured, 5 mm) and horizontal wind velocities (vector, 3 ms^{-1}) for 17-18 June

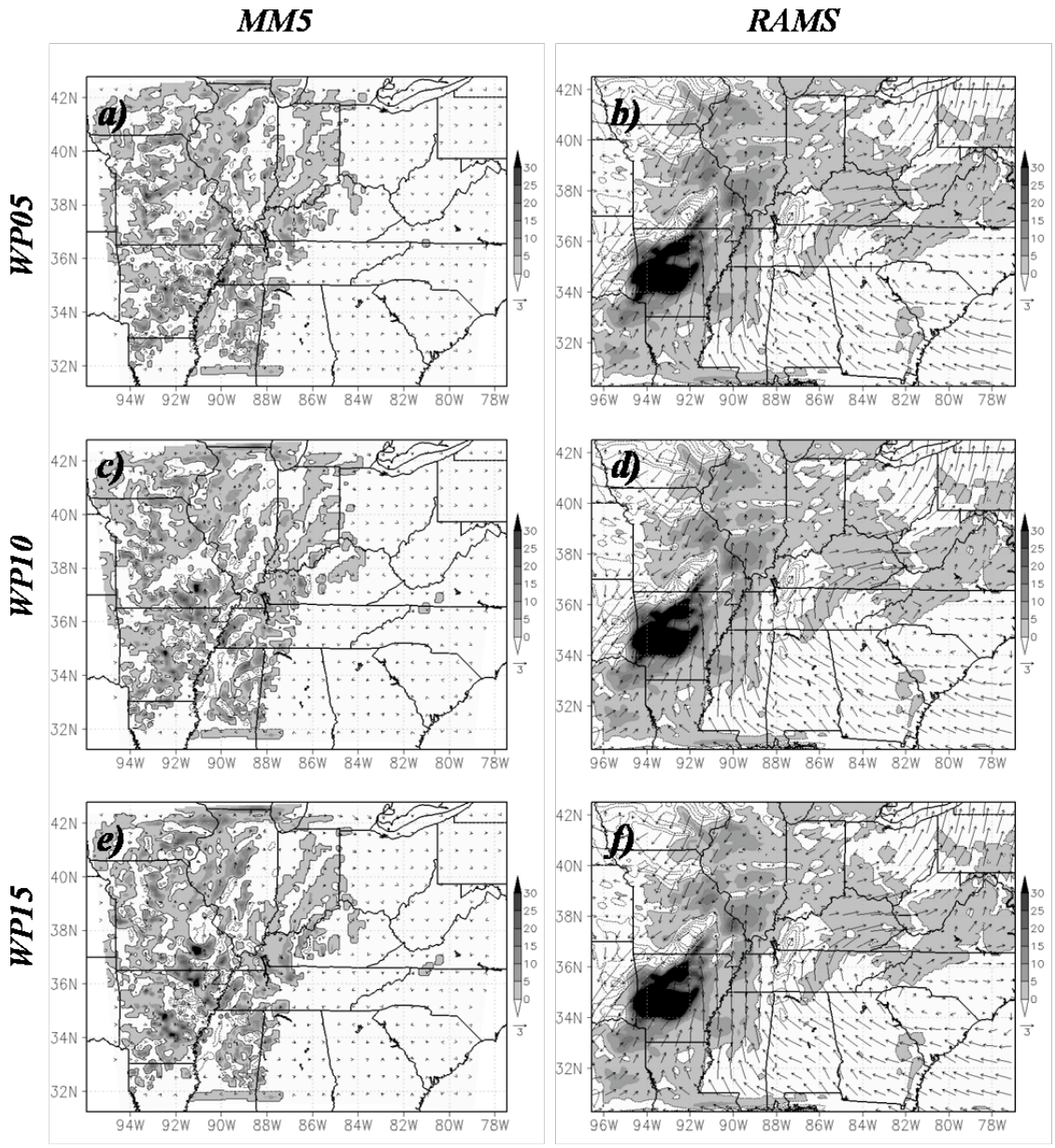

Figure 16, MM5 and RAMS wet experiment minus CTRL precipitation (positive values shaded according to scale, negative values contoured, 5 mm) and horizontal wind velocities (vector, 3 ms^{-1}) for 17-18 June

produced less precipitation with the strongest gradient between the experiment and CTRL.

MM5 2 m horizontal wind fields were not very sensitive to positive or negative perturbations of soil moisture. Neither wet nor dry experiments presented significant differences with respect to CTRL. Only in regions where the precipitation maxima were displaced, small changes in 2 m wind speeds could be observed. For example, MM5 WP15 presented horizontal wind speed greater than 1 m s^{-1} with respect to CTRL. Furthermore, the 2 m horizontal wind field was affected by the displacement of precipitation in RAMS simulations. Increases and decreases of SM resulted in an overall displacement of the horizontal wind fields. As seen in Figure 15 and 16, the largest wind speed differences between the experiments and CTRL corresponded to the regions where the largest precipitation gradients were found.

Equivalent Potential Temperature

As seen in Figure 17, MM5 dry simulations did not significantly varied from CTRL run. DP05 and DP10 produced θ_e values of 1 and 2 K respectively. The maxima were located at 86°W and 83°W longitude respectively for the experiments.

On the other hand, WP15 produced θe values of 3 K located at 700 hPa and extending from 84°W to 81°W longitude. Wet experiments were also characterized by small differences between the experiments and CTRL. WP05 and WP10 produced θe temperatures 2 K greater than CTRL. A small region of increased θe at 900 hPa could be found around 80°W for all experiments. WP15 presented an additional region of increase θe at 900 hPa located at 90°W.

The effect of misplaced precipitation in RAMS simulation can also be observed with respect to θe. As seen in Figure 17 (b, d, f), negative perturbations of SM resulted in lower values of θe near the surface. On the other hand, a strong θe gradient can be observed at 700 hPa from 89°W to 82°W longitude. Near the surface, the western region of DP15 domain is characterized by values of θe less than 7 K, while the eastern section of the domain was characterized by θe greater than 6 K.

3-D Vertical Wind

Figure 19 summarizes the 3-D modeled wind disparities between each dry experiment and CTRL respectively for 18 June. Examinations of each MM5 simulation reveal that for this event, decreases of SM were conducive of increased vertical wind speeds. MM5 DP05 produced the strongest vertical wind with

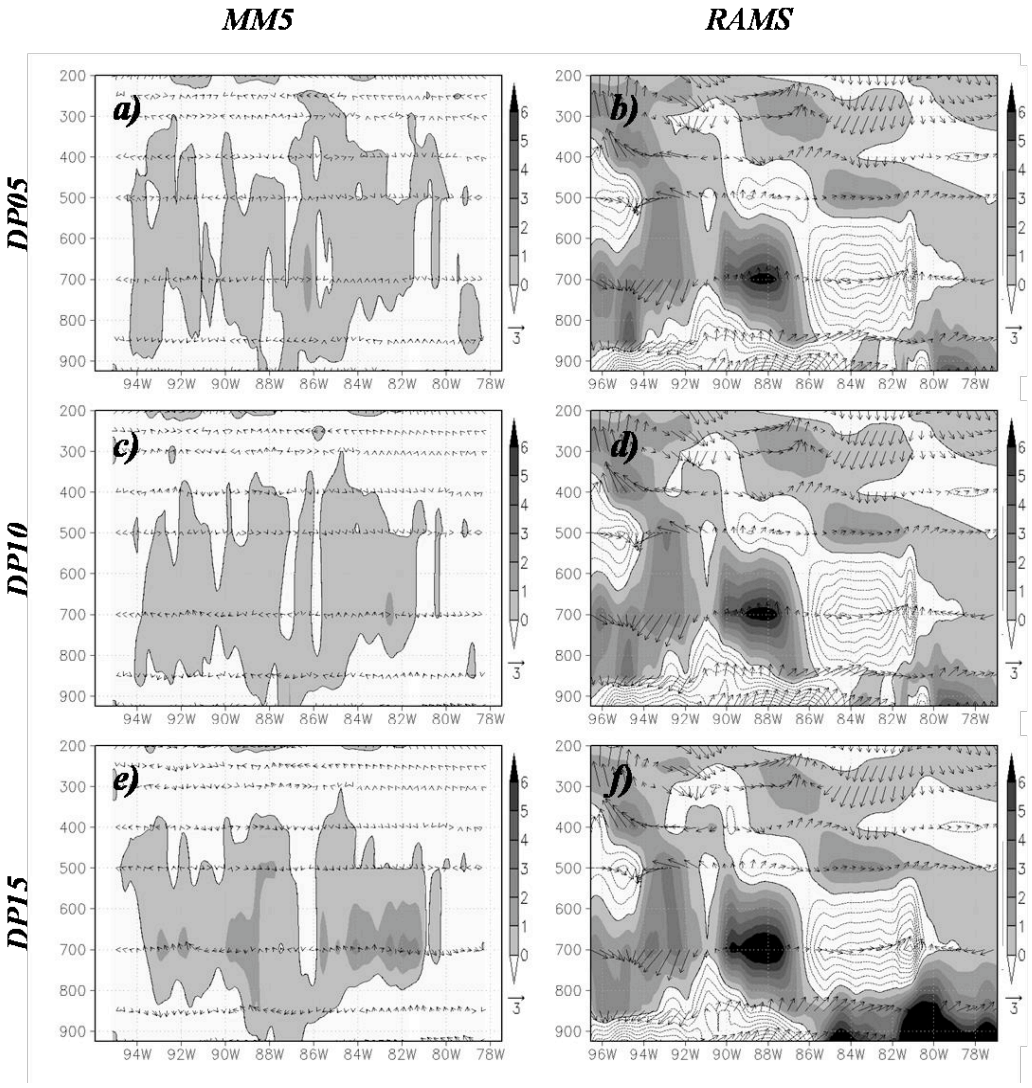

Figure 17. MM5 and RAMS dry experiment minus CTRL cross-sections of 12-h averaged equivalent potential temperature (positive values shaded according to scale, negative values contoured, K) and horizontal wind velocities (vector, 3 ms^{-1}) for 94°W to 78°W longitude and 37°W latitude centered at 0000 UTC on 18 June

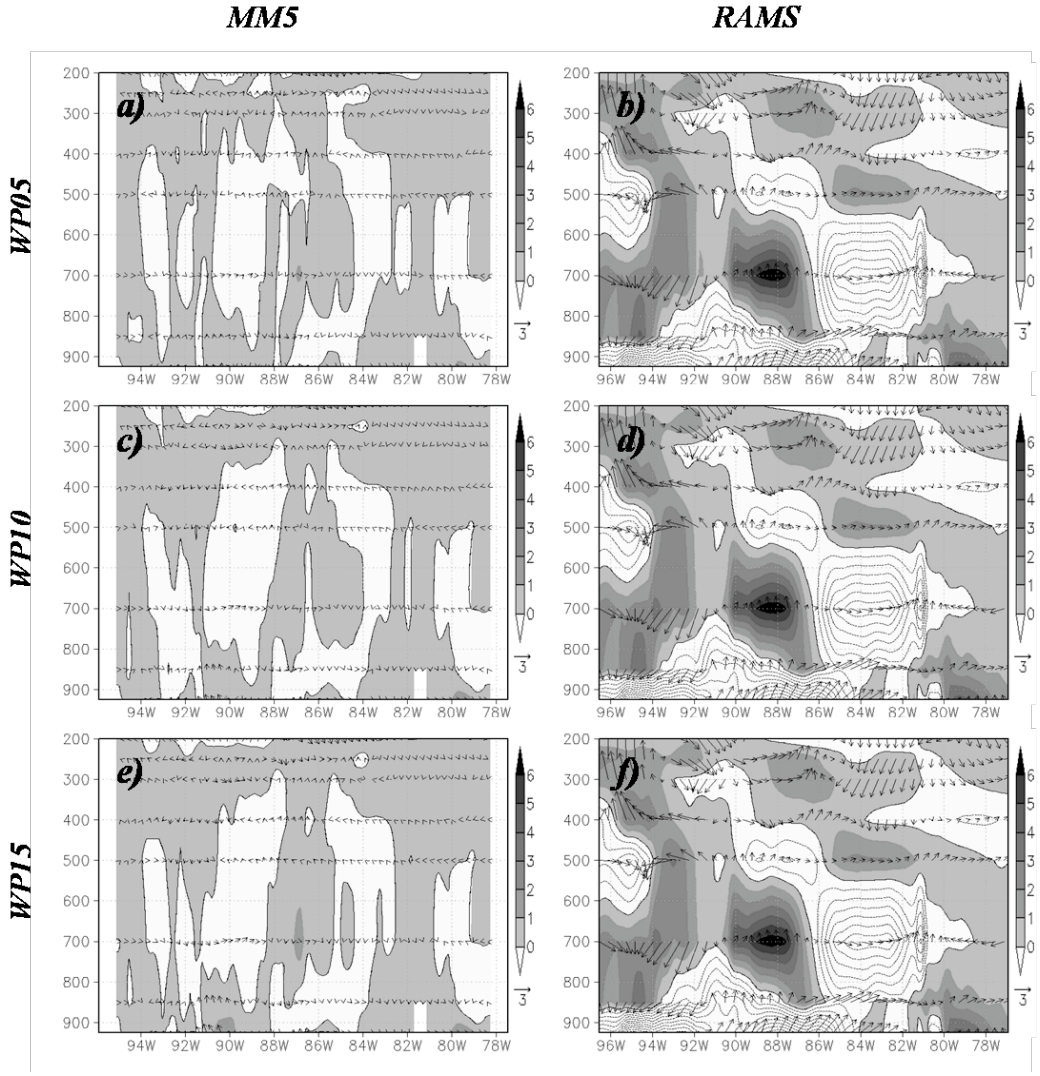

Figure 18. MM5 and RAMS wet experiment minus CTRL cross-sections of 12-h averaged equivalent potential temperature (positive values shaded according to scale, negative values contoured, K) and horizontal wind velocities (vector, 3 ms^{-1}) for 94°W to 78°W longitude and 37°W latitude centered at 0000 UTC on 18 June

vertical motions of up to 12 cm s^{-1} with respect to CTRL located at 92°W longitude.. This strong column of vertical velocities extended from the surface up to 300 hPa. On the other hand, positive perturbation of SM resulted on increased vertical velocities for all wet simulations with maxima greater than 0.12 cm s^{-1} located at 92°W longitude, where a precipitation maximum can be found at 37°N latitude.

Furthermore, RAMS precipitation displacement can also be noted while examining the 3-D modeled wind velocities. All experiments (Figure 19 and 17b, d, f) displayed a strong gradient extending from 93°W to 91°W longitude. Regions, in which the experiments produces higher wind speeds than CTRL, correspond to the southeastward displacement of precipitation. Little variation is observed among the experiments with respect to vertical speeds and maxima locations. Both wet and dry experiment positioned a vertical velocity minimum with respect to CTRL at 92°W longitude. This minimum was surrounded by a maximum to the east and west.

Latent Heat Flux

As expected for MM5, negative perturbations of SM resulted in

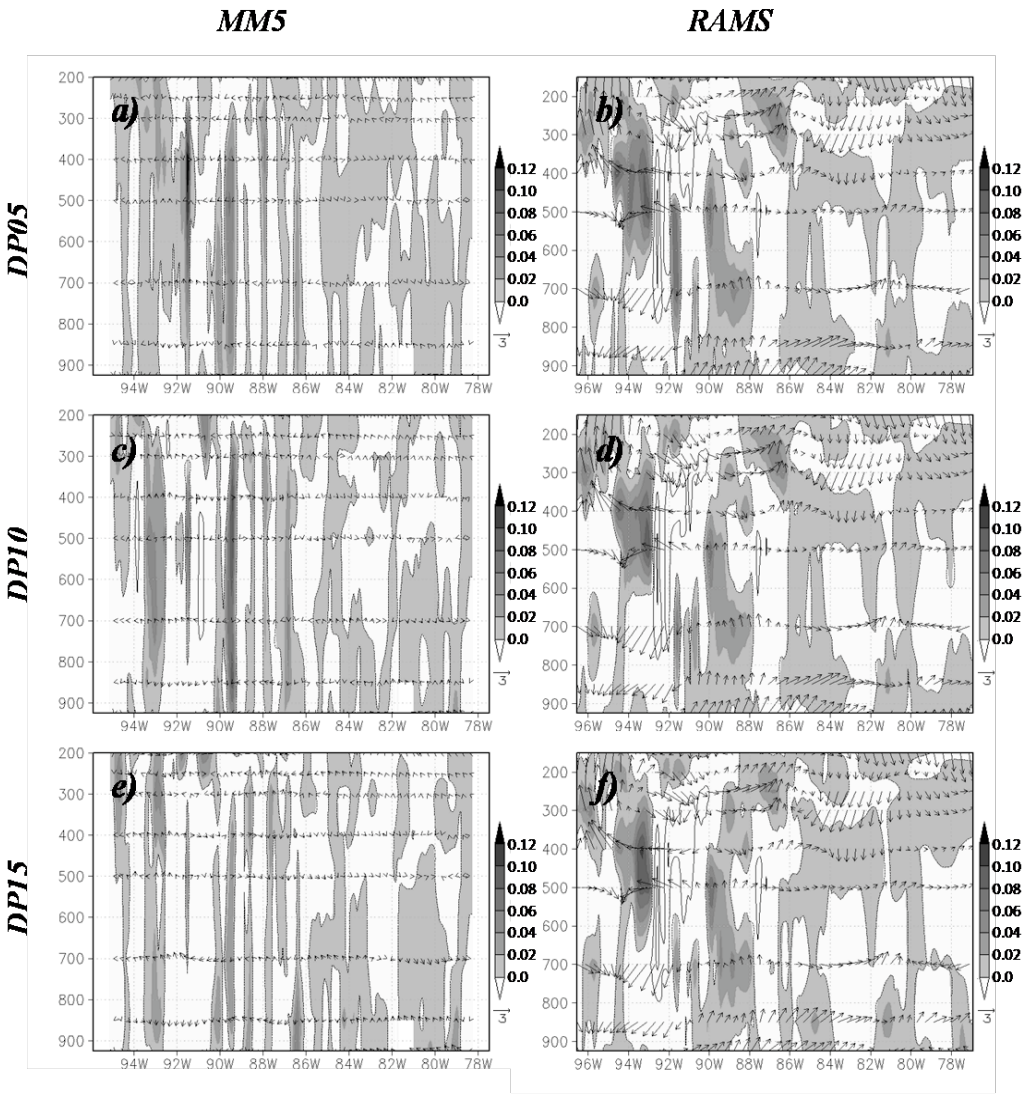

Figure 19. MM5 and RAMS dry experiment minus CTRL cross-sections of vertical wind profile (positive values shaded according to scale, negative values contoured, 0.02 ms^{-1}) and horizontal wind velocities (3 ms^{-1}) for 94°W to 78°W longitude and 37°W latitude centered at 0000 UTC on 18 June

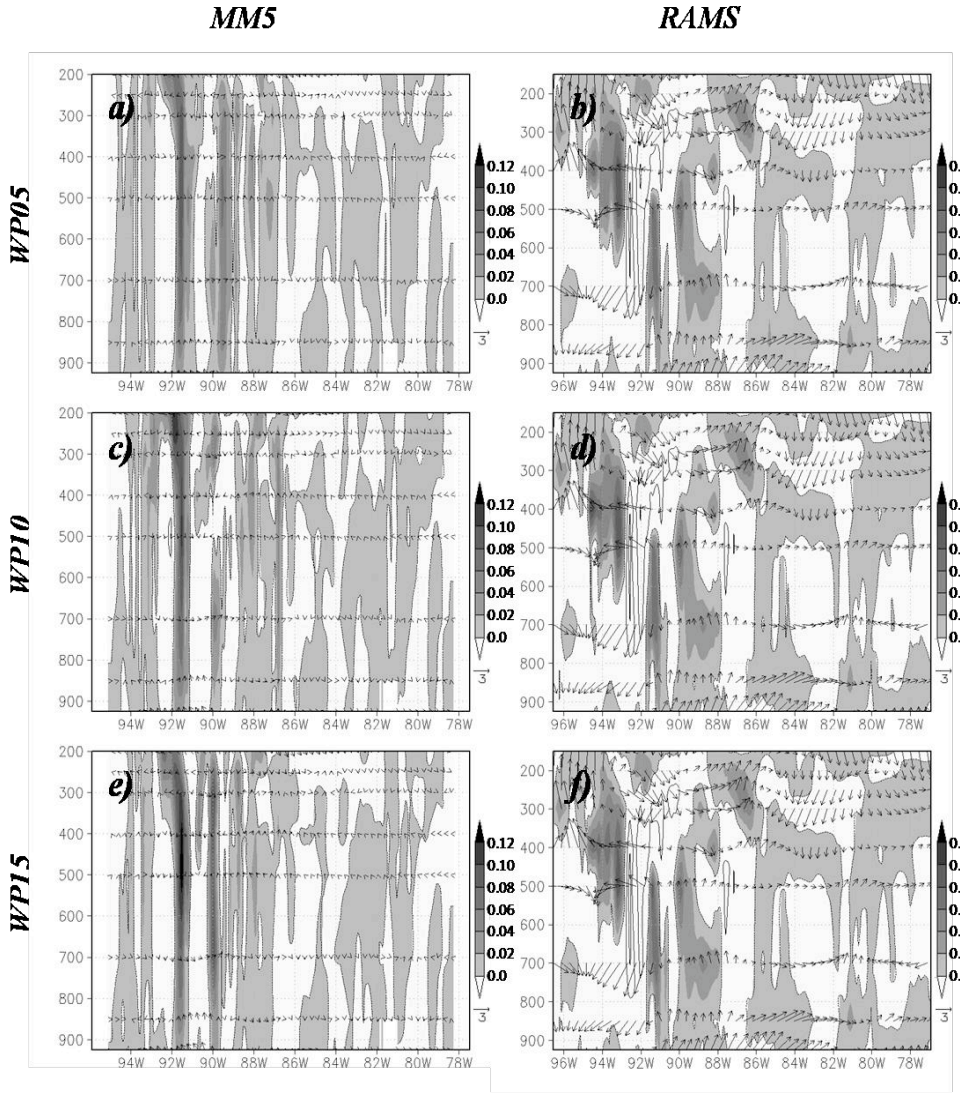

Figure 20. MM5 and RAMS dry experiment minus CTRL cross-sections of vertical wind profile (positive values shaded according to scale, negative values contoured, 0.02 ms^{-1}) and horizontal wind velocities (vector, 3 ms^{-1}) for 94°W to 78°W longitude and 37°W latitude centered at 0000 UTC on 18 June

decreased latent heat flux through the study region compare to CTRL. As seen in Figure 21a, a 0.05 m^3m^{-3} decrease of SM induced latent heat fluxes minima and maxima of more than 100 Wm^{-2} with respect to CTRL over the western region of the domain. However, MM5 DP10 and DP15 experienced small latent heat flux variations with respect to CTRL. MM5 wet experiments were generally characterized by positive latent heat fluxes compared to CTRL.

Sharp latent heat flux gradients can be observed for RAMS wet and dry experiment. This gradient can be attributed to the displacement of the precipitation observed on RAMS experiments. CTRL experiment produced up to 120 Wm^{-2} greater latent heat flux compared to DP05, DP10, and DP15 sensitivity experiments over large regions. These maxima are mainly located over the eastern portion of the domain. WP05, WP10, and WP15 also showed the displacement of precipitation over the central regions of the domain. Wet experiments had less of an impact on the latent heat flux, with little to no variation among the simulations.

Sensible Heat Flux

MM5 dry experiments were highly sensitive to SM perturbations when resolving sensible heat flux. As seen in Figure 23, decreases in SM resulted in

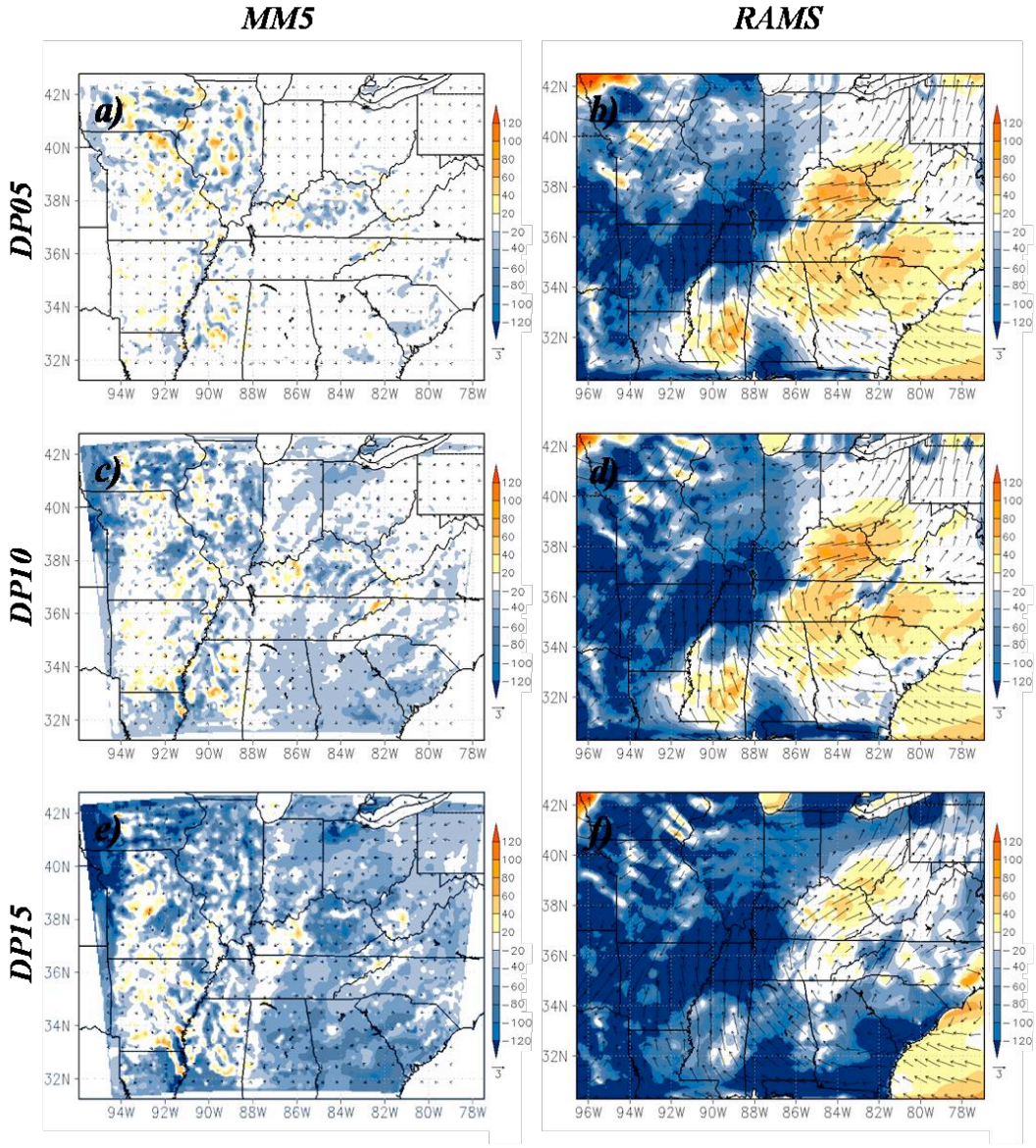

Figure 21. MM5 and RAMS dry experiment minus CTRL of 12-h averaged latent heat fluxes (shaded according to scale, 40 m) and horizontal wind velocities (vector, 3 ms^{-1}) centered at 0000 UTC on 18 June.

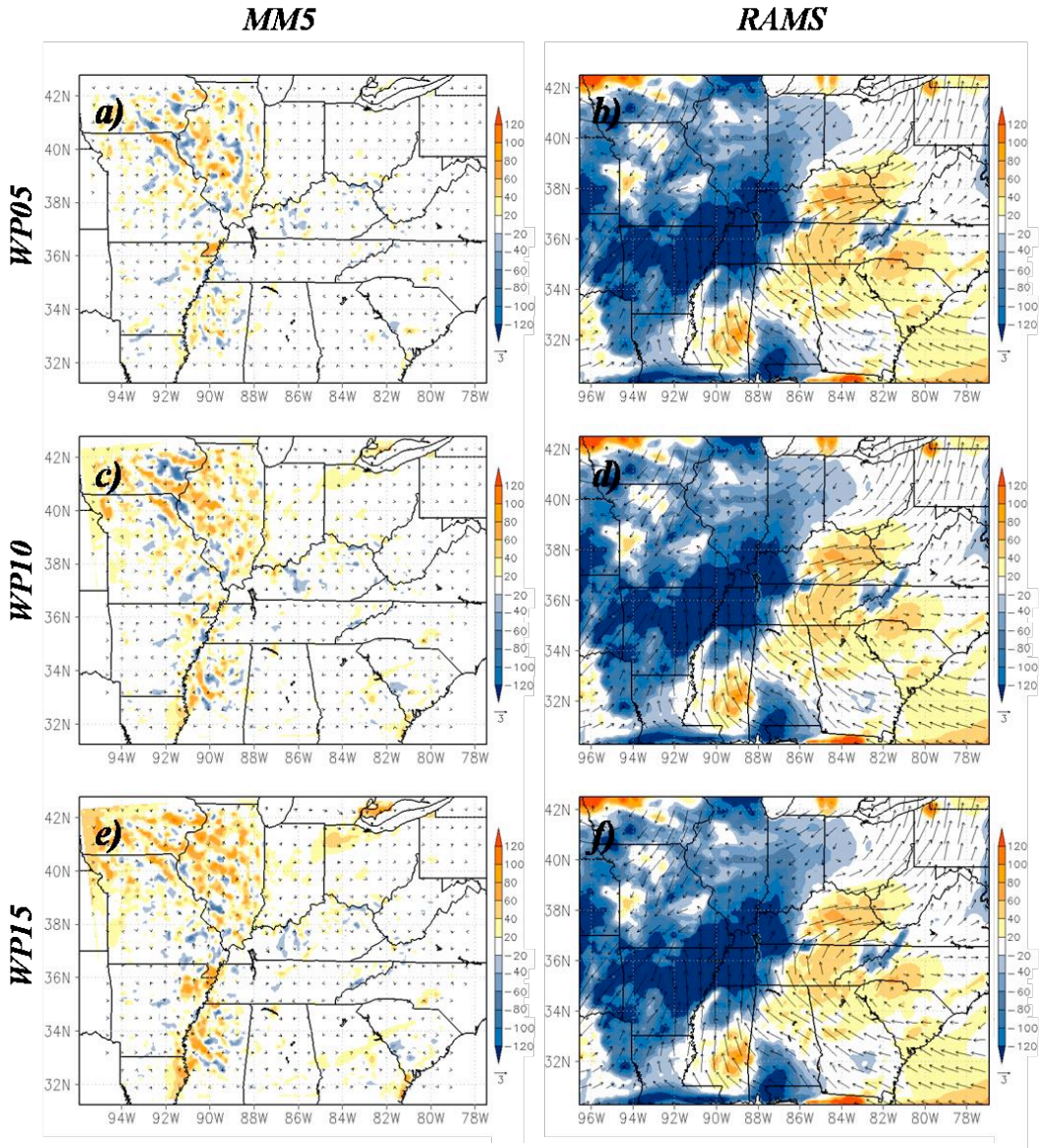

Figure 22. MM5 and RAMS wet experiment minus CTRL of 12-h latent heat fluxes (shaded according to scale, 40 m) and horizontal wind velocities (vector, 3 ms^{-1}) centered at 0000 UTC on 18 June

increased sensible heat flux. DP05 produced small regions along the Mississippi River and the Missouri-Illinois border, in which the experiment resolved greater sensible heat fluxes than CTRL. Decreases in SM resulted in regions where DP10 and DP15 experienced sensible heat fluxes greater than 120 Wm^{-2} with respect to CTRL. Wet experiments, on the other hand, produced little to no variation of sensible heat flux with respect to CTRL as seen in Figure 24a, c, e. WP05, WP10, and WP15 resolved narrow area along the Mississippi River in which the experiments produced up to 40 Wm^{-2} than CTRL.

RAMS dry and wet experiments for 17-18 June presented more variability of sensible heat fluxes than MM5. These experiments are summarized in Figures 23 and 24. RAMS DP05, DP10, and DP15 increasingly resolved larger areas in which the experiments resolved higher values of sensible heat flux. Due to the displacement of precipitation, an area located over Arkansas, western Tennessee and Kentucky can be found in which decreases in SM resulted in decreases sensible heat for dry experiments with respect to CTRL. Wet simulations were less sensitive to increases in SM when resolving sensible heat flux.

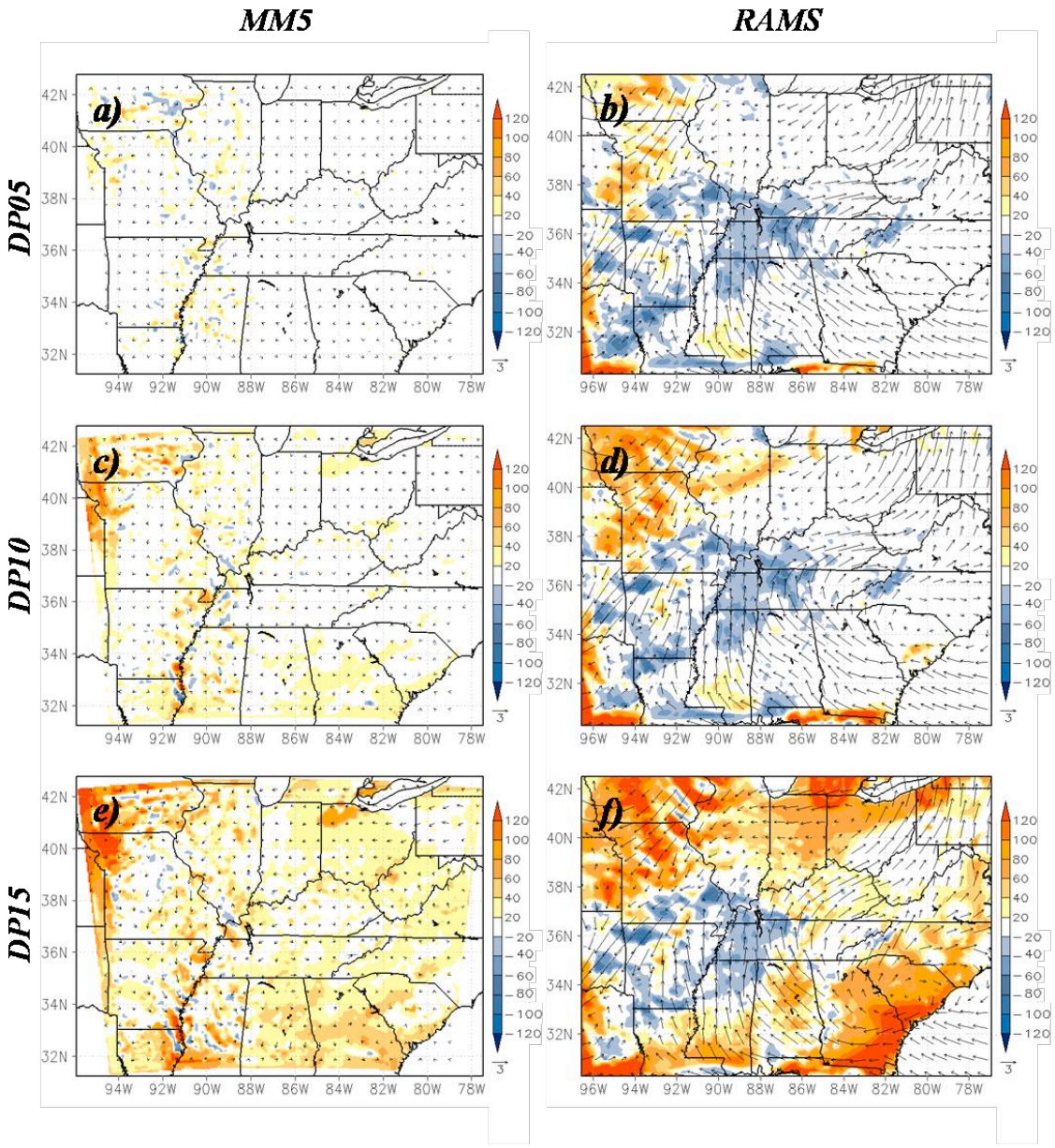

Figure 23. MM5 and RAMS dry experiment minus CTRL of 12-h averaged sensible heat fluxes (shaded according to scale, 40 m) and horizontal wind velocities (vector, 3 ms^{-1}) centered at 0000 UTC on 18 June.

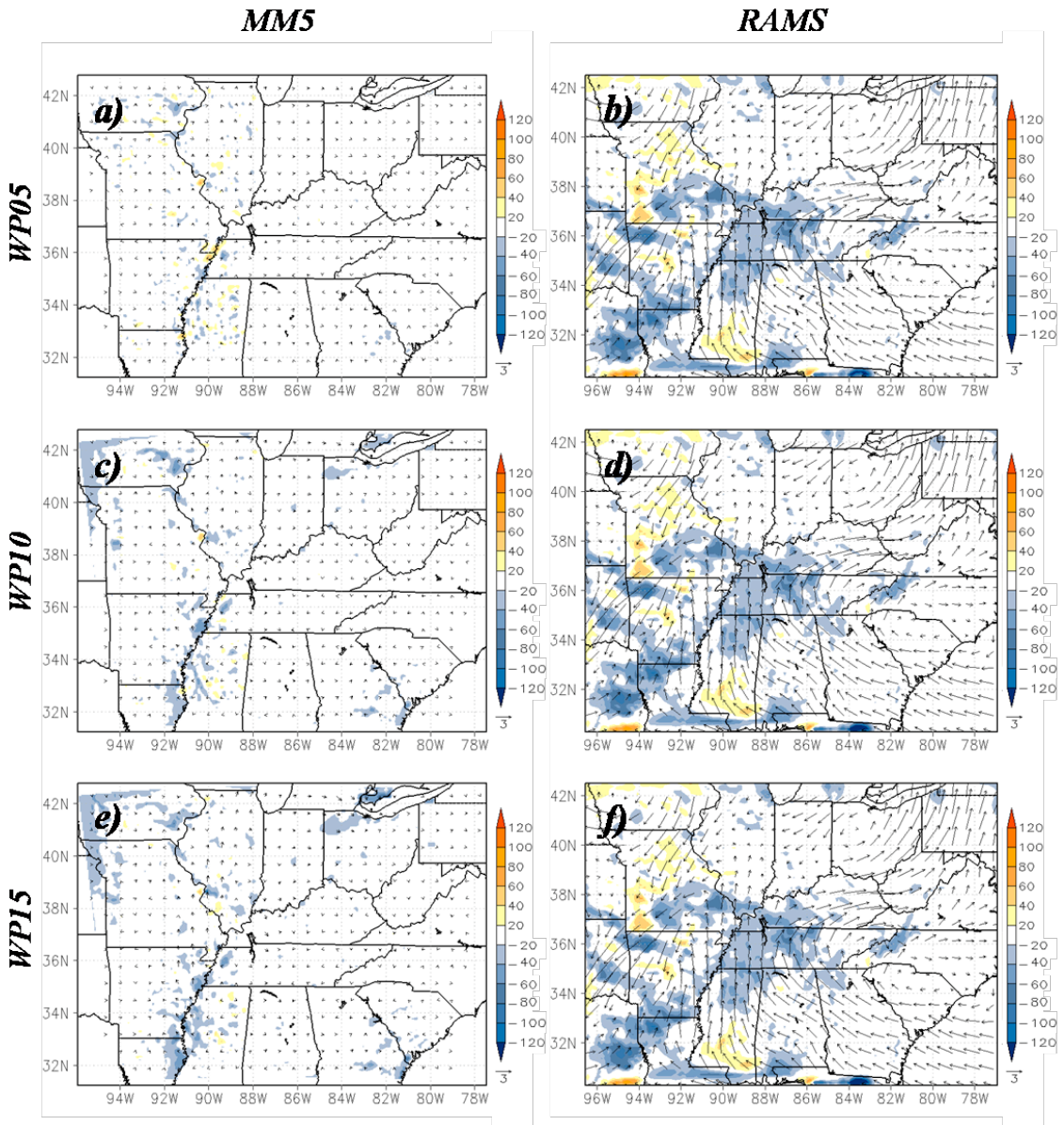

Figure 24. MM5 and RAMS wet experiment minus CTRL of 12-h averaged sensible heat fluxes (shaded according to scale, 40 m) and horizontal wind velocities (vector, 3 ms^{-1}) centered at 0000 UCT on 18 June.

21-22 June 2006

Precipitation and Horizontal Wind

Negative perturbations of SM, once again, were conducive of decrease precipitation for MM5 simulations. DP05, DP10, and DP15 simulated a region of increased precipitation over Indiana and northern Ohio. These maxima were coupled with region of decreased precipitation for all experiments with respect to CTRL. DP15 resolved displacement of precipitation over Missouri and Illinois. The precipitation gradient on the area revealed that the precipitation maximum present in CTRL was displaced eastward for this experiment. On the other hand, wet experiments simulated precipitation quantities greater than 5 mm with respect to CTRL for most of the domain. Precipitation maxima were located over the northern section of the event extending from Missouri to northern Ohio. The displacement of precipitation was mostly noted on WP05 and WP10 experiments over northern Indiana and Ohio. Overall, positive perturbations of SM resulted in increased precipitation accumulations for MM5.

RAMS dry simulations transposed the precipitation maximum northwest with respect to CTRL, as seen in Figure 25. RAMS dry experiments position the

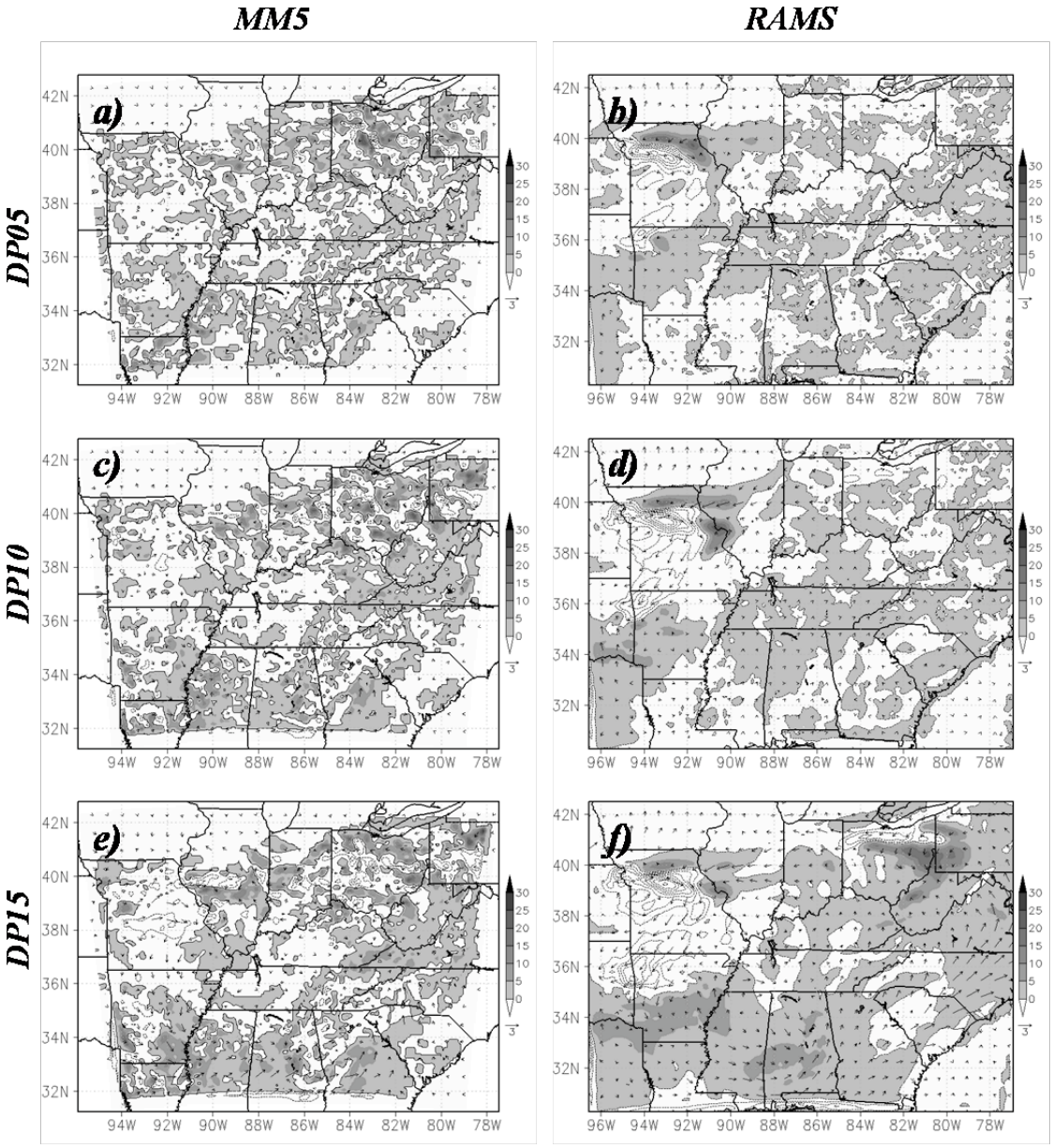

Figure 25. MM5 and RAMS dry experiment minus CTRL precipitation (positive values shaded according to scale, negative values contoured, 5 mm) and horizontal wind velocities (vector, 3 ms^{-1}) for 22-23 June

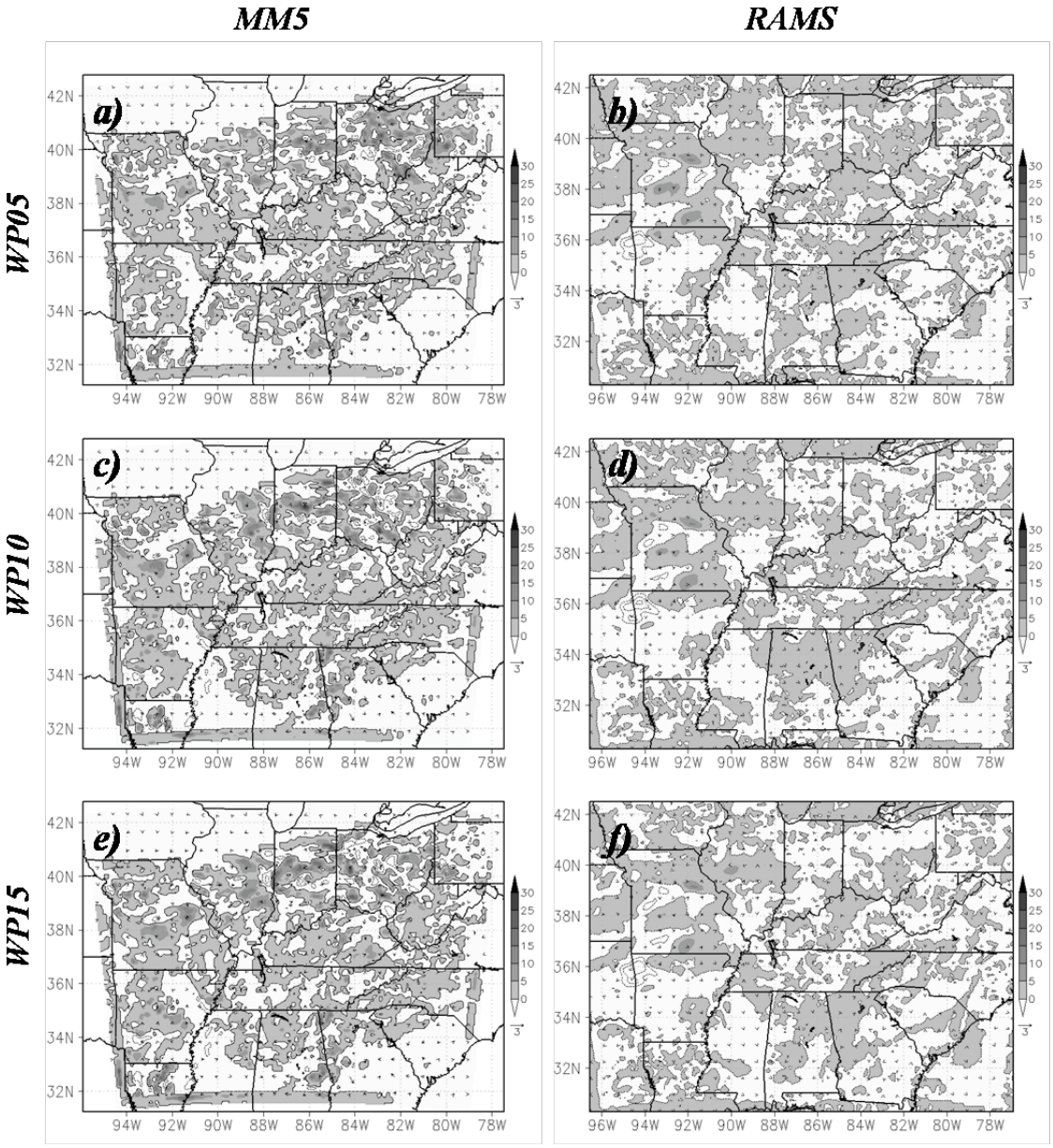

Figure 26. MM5 and RAMS wet experiment minus CTRL precipitation (positive values shaded according to scale, negative values contoured, 5 mm) and horizontal wind velocities (vector, 3 ms^{-1}) for 22-23 June

precipitation maxima over the Missouri and Illinois border. A strong sharp gradient can be observed in Figure 25 (b, d, and f) slightly southwestward of the experiment maxima, where the CTRL maximum was located. In addition, DP15 experiment resolved a precipitation maximum over northern Ohio as a result of precipitation displacement as well. Overall, decreases in SM resulted in decreased precipitation accumulation and greater precipitation displacement. Wet experiments on the other hand were less sensitive to SM perturbations. WP05, WP10, and WP15 produced large areas in which the accumulated precipitation difference between the experiments and CTRL did not exceed 5 mm.

MM5 wet and dry experiments did not simulated significant 2 m horizontal wind velocities disparities between the experiments and the CTRL (Figure 25 and 26). Both sets of experiments resolved similar wind speed patterns with respect to CTRL despite the displacement of precipitation. Furthermore, RAMS dry and wet simulations did not produce large wind speed disparities with respect to CTRL. For dry experiments, the maximum differences of horizontal wind velocities were located in region of precipitation displacement (i.e. northern Missouri and Ohio) with respect to CTRL. 2 m horizontal wind speeds did not varied by more than 1, 3, and 3.2 m s^{-1} for DP05, DP10, and DP15, respectively. Overall, decreases in SM

resulted in horizontal displacement of precipitation, thus increases of horizontal wind velocities. Positive perturbations of SM did not have any notable impacts on the 2 m horizontal wind velocities.

Equivalent Potential Temperature

θ_e varied significantly among the individual experiments for MM5 dry and wet experiments. Figure 27 showed the difference between the dry experiments and CTRL. MM5 DP05 experiment did not produce θ_e greater than 2 K compared to CTRL. DP10 and DP15 resolved θ_e values 3 and 6 K greater than CTRL. These θ_e maxima were found at 700 hPa and positioned at 92°W and 80°W longitude; they marked the top of the PBL layer which is characterized by strong differences of θ_e. Wet experiments, on the other hand, did not produce significant differences of θ_e values with respect to CTRL. The effect of increase in SM on wet experiments can best be observed at 900 hPa where small maxima developed at 90°W and 80°W longitude for WP15. Overall, increases in SM resulted in θe changes less than 1 K compared to CTRL.

Decreases in SM, resulted in modified θ_e for RAMS dry experiments with respect to CTRL (Figure 27). DP05 produced a region of increased θ_e at 900 hPa

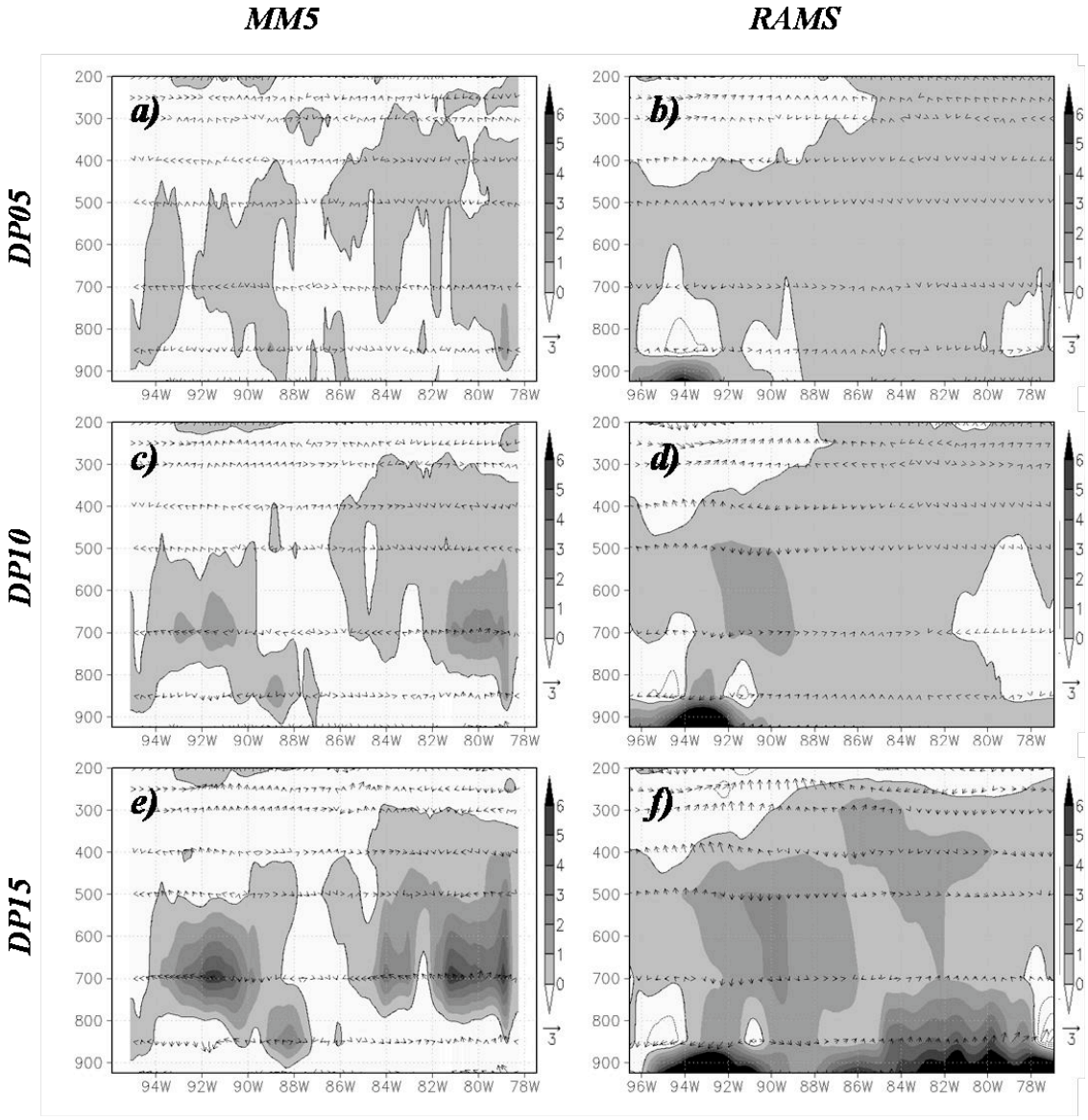

Figure 27. MM5 and RAMS dry experiment minus CTRL cross-sections of 12-h averaged equivalent potential temperature (positive values shaded according to scale, negative values contoured, K) and horizontal wind velocities (vector, 3 ms^{-1}) for 94°W to 78°W longitude and 37°W latitude centered at 0000 UTC at 23 June

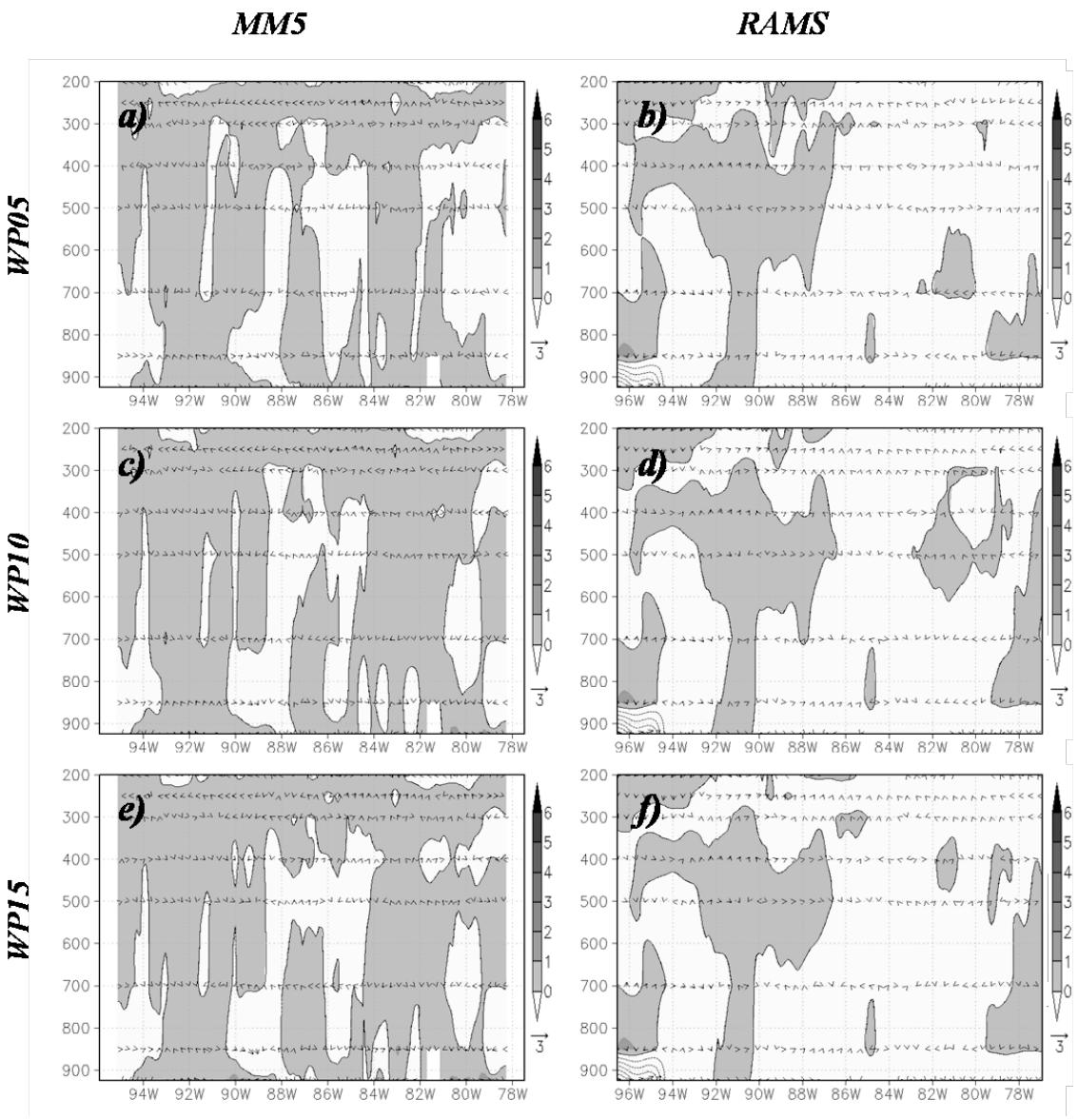

Figure 28. MM5 and RAMS wet experiment minus CTRL cross-sections of 12-h averaged equivalent potential temperature (positive values shaded according to scale, negative values contoured, K) and horizontal wind velocities (vector, 3 ms^{-1}) for 94°W to 78°W longitude and 37°W latitude centered at 0000 UTC on 23 June

around 94°W longitude. The same region experienced increased θ_e values with decreased SM for DP10 and DP15 with respect to CTRL. DP15 also resolved greater θ_e at 900 hPa between 83°W to 77°W longitudes versus CTRL. Positive perturbations of SM produced little variation between WP experiments and CTRL. WP05, WP10, and WP15 experienced θ_e values less than 1 K compared to CTRL (Figure 28 b, d, and f). On the other hand, RAMS wet experiments produced significantly lower values of θ_e over the western section of the domain, where CTRL produced up to 5 K more than each wet experiment.

3-D Vertical Wind

Figure 29 summarized 12-h averaged vertical wind velocities centered at 0000 UCT 22 June. Decreases in SM produced increased vertical wind velocities at 84°W longitudes. This feature could be seen in DP10 and DP15 which produced vertical winds velocities greater than 0.08 and 0.10 cm s^{-1}, respectively, in comparison with CTRL. On the other hand, decreases of SM increased vertical wind velocities for WP05, (Figure 30a). This sensitivity test event produced vertical wind velocities of up to 0.08 cm s^{-1} with respect to CTRL. Further increases of SM did not result in increased vertical wind velocities for WP10 and WP15, although the

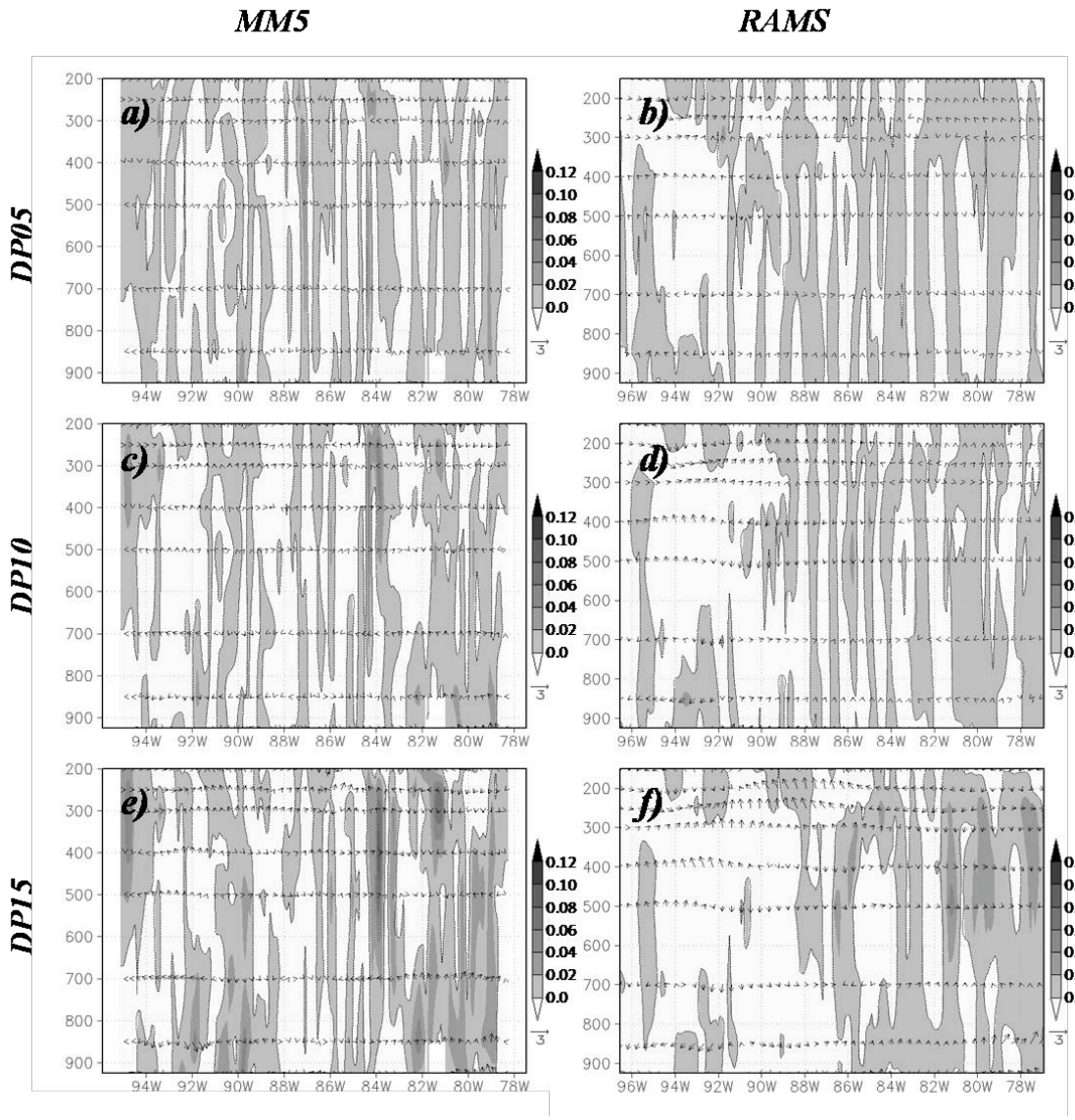

Figure 29. MM5 and RAMS dry experiment minus CTRL cross-sections of vertical wind profile (positive values shaded according to scale, negative values contoured, 0.02 ms^{-1}) and horizontal wind velocities (vector, 3 ms^{-1}) for 94°W to 78°W longitude and 37°W latitude centered at 0000 UTC on 23 June

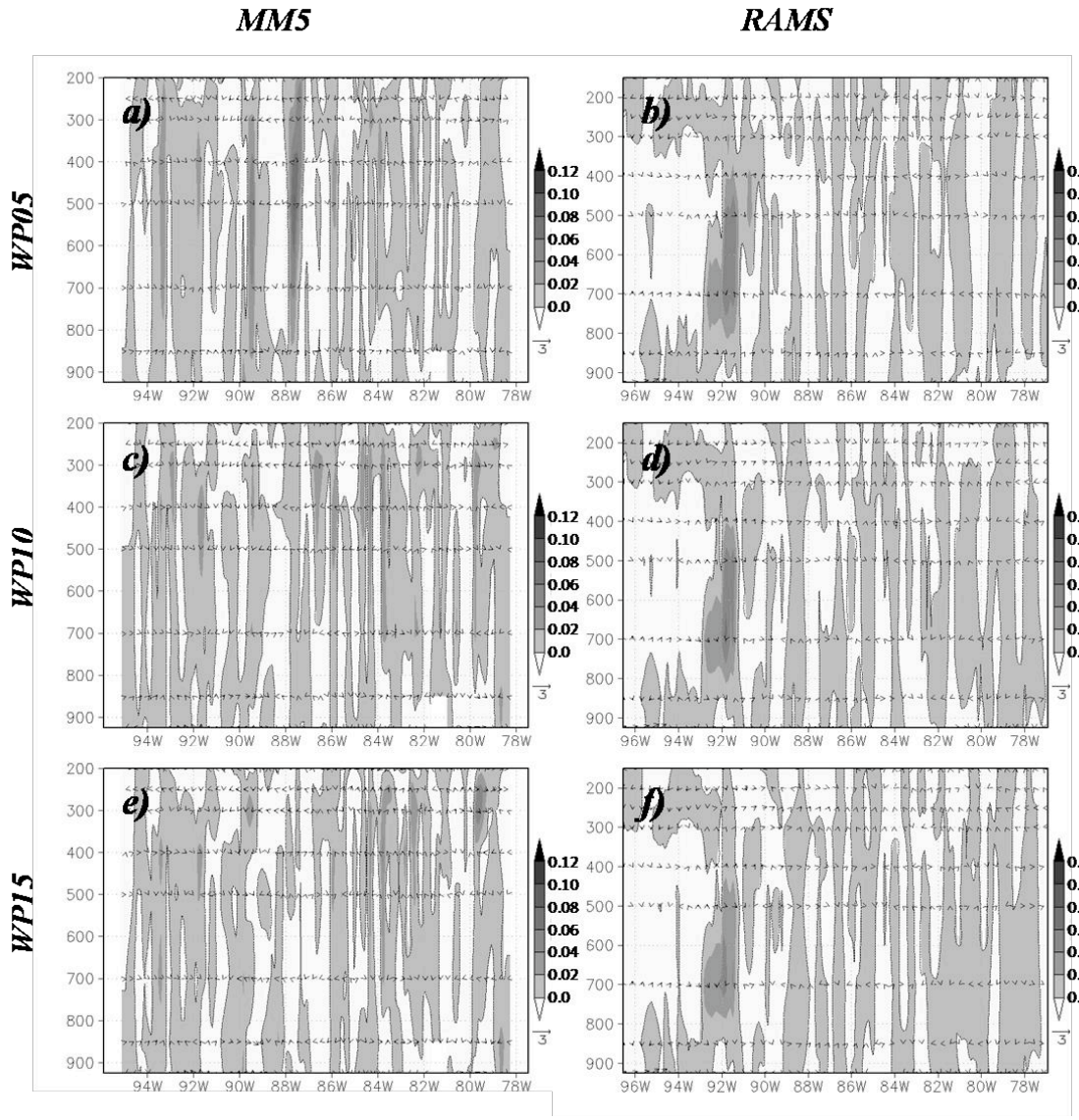

Figure 30. MM5 and RAMS dry experiment minus CTRL cross-sections of vertical wind profile (positive values shaded according to scale, negative values contoured, 0.02 ms^{-1}) and horizontal wind velocities (vector, 3 ms^{-1}) for 94°W to 78°W longitude and 37°W latitude centered at 0000 UTC on 23 June

event experienced increases of up to 0.04 ms^{-1} versus CTRL.

3-D vertical wind estimated by RAMS wet and dry experiments responded somewhat similarly compared to MM5 simulations. Decreases in SM resulted in increased vertical velocities for the eastern section of the domain. DP15 produced vertical wind velocities 0.06 cm s^{-1} greater than CTRL at 81°W longitude. However, increase in SM also resulted in increase in vertical velocities greater than 0.06 cm s^{-1} compared to CTRL for WP05 and WP10 sensitivity tests.

Latent Heat Flux

Differences of 12-h averaged latent heat fluxes centered at 0000 UTC 22 June between dry experiments and CTRL were shown in Figure 31. MM5 dry experiments revealed that increases in SM resulted in an overall decrease of latent heat fluxes. SM negative perturbation of 0.05 m^3m^{-3} did not have significant impact on the latent heat fluxes. On the other hand, as the soil was further dried DP10 and DP15, latent heat fluxes differences increased up to -120 Wm^{-2} with respect to CTRL. As seen in Figure 32, the simulations were less sensitive to increases of SM.

RAMS dry experiments produced large regions of negative latent heat fluxes. Overall, decreases of SM resulted in decreases less than -120 Wm^{-2} with respect to

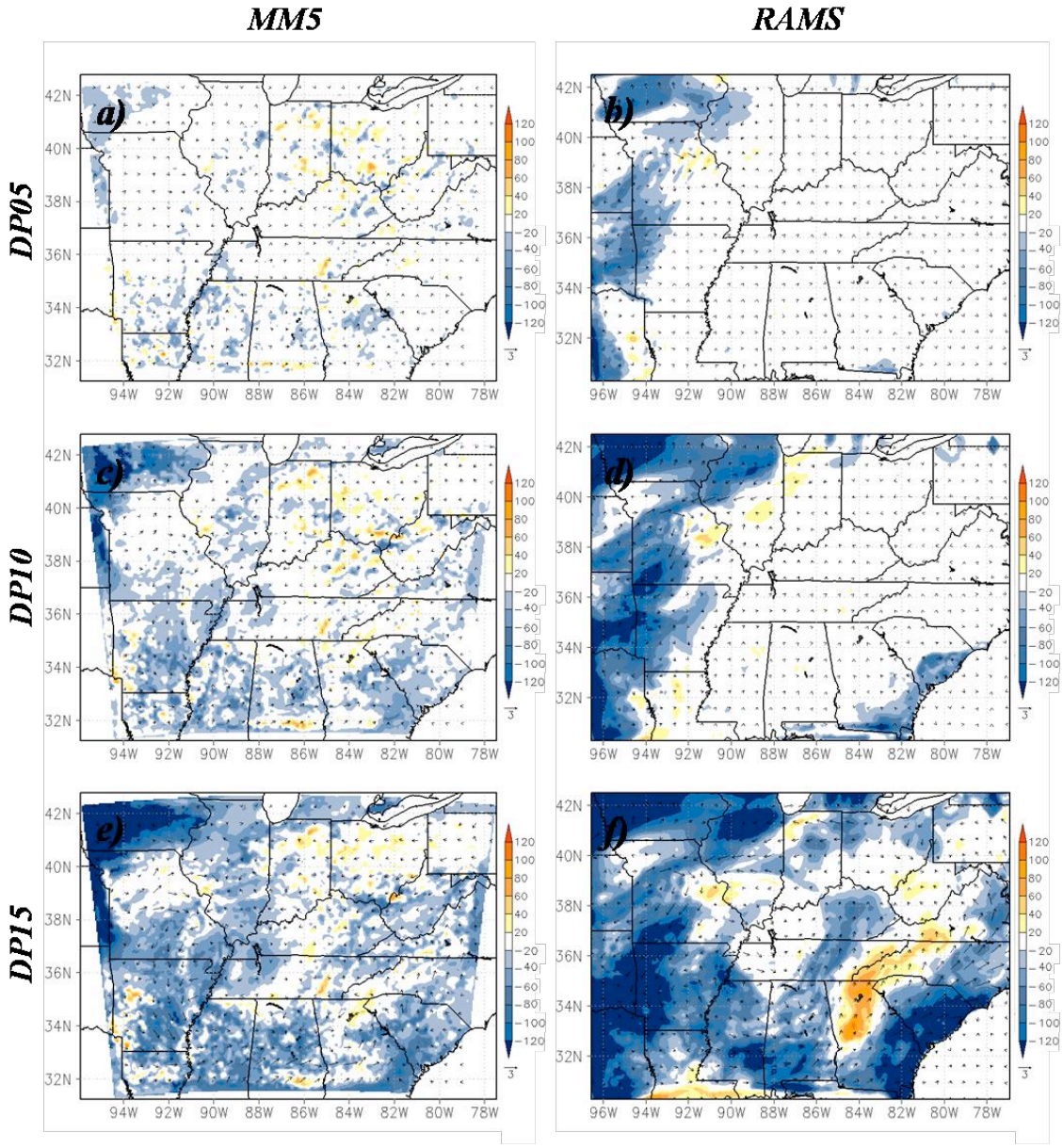

Figure 31. MM5 and RAMS dry experiment minus CTRL of 12-h averaged latent heat fluxes (shaded according to scale, 40 m) and horizontal wind velocities (vector, 3 ms^{-1}) centered at 0000 UTC on 23 June.

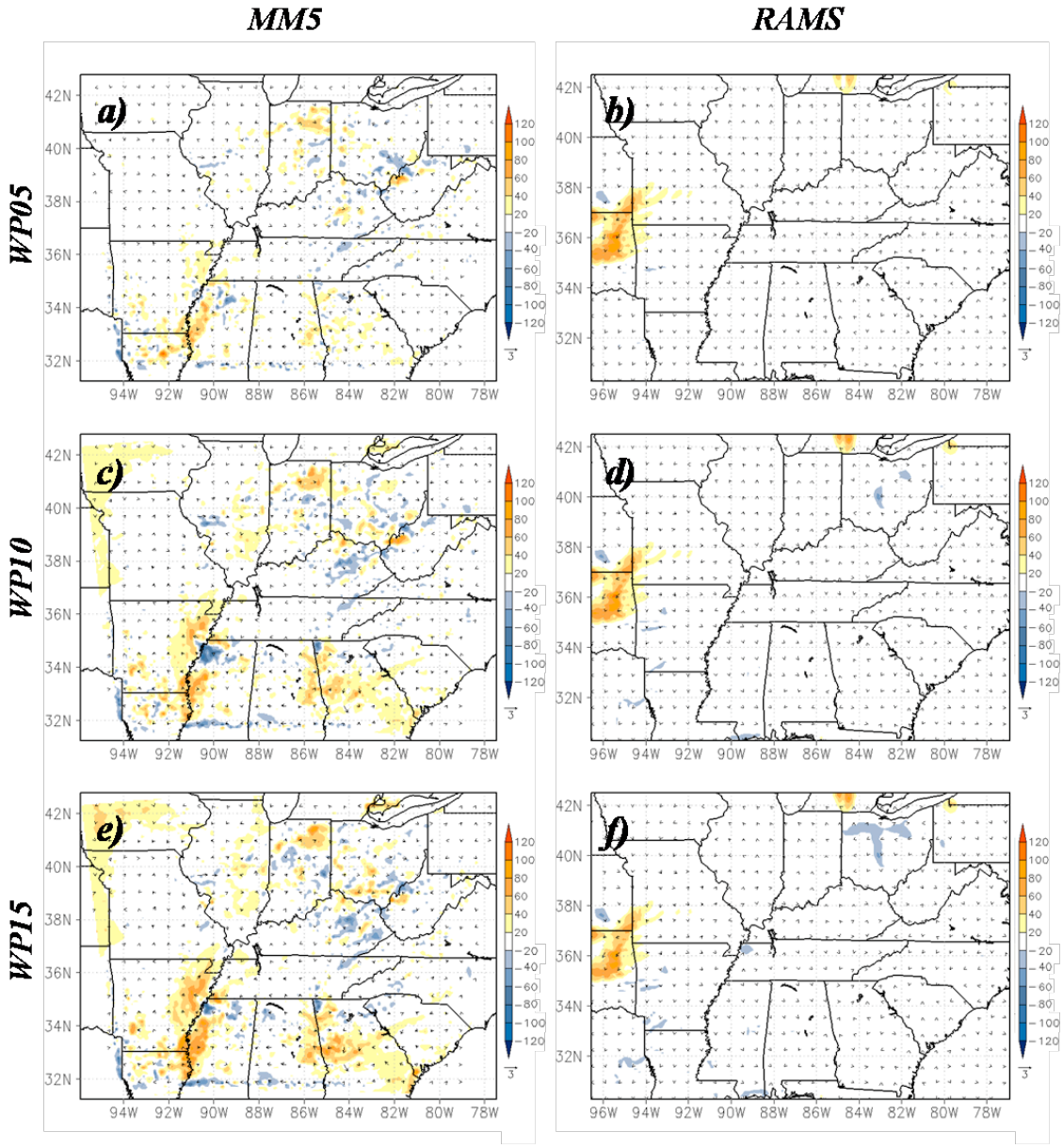

Figure 32. MM5 and RAMS wet experiment minus CTRL of 12-h averaged latent heat fluxes (shaded according to scale, 40 m) and horizontal wind velocities (vector, 3 ms^{-1}) centered at 0000 UTC on 23 June.

CTRL for DP05, DP10, and DP15. DP15, however, developed a region of increased latent heat fluxes with decreased SM over Georgia and eastern North Carolina. The maximum presented fluxes greater than 100 Wm^{-2} versus CTRL. As seen in Figure 32 b, d, and f, positive perturbations of SM resulted in increased latent heat fluxes over eastern Oklahoma for all three experiments. Although, WP05 and WP10 produced the largest fluxes 100 W m^{-2} compared to CTRL. .

Sensible Heat Flux

Figure 33 and 34 summarized averaged 12-h difference of sensible heat fluxes for wet and dry experiments with respect to CTRL, respectively. Figure 32a revealed that SM decreases of 0.05 m^3m^{-3} did not produce significant differences between DP05 and CTRL. DP10 and DP15 produced regions were positive sensible heat fluxes exceeded 120 Wm^{-2} over Iowa. Positive perturbation of SM, however, produced little to no variation for all three simulations. WP10 and WP15 presented -20 Wm^{-2} over the western section of the domain and the Mississippi River Valley.

RAMS dry experiments positioned a positive sensible heat flux maxima over southern Iowa. These maxima encompassed fluxes greater than 120 Wm^{-2} for all three simulations. In addition, DP10 and DP15 sensible heat flux simulations versus

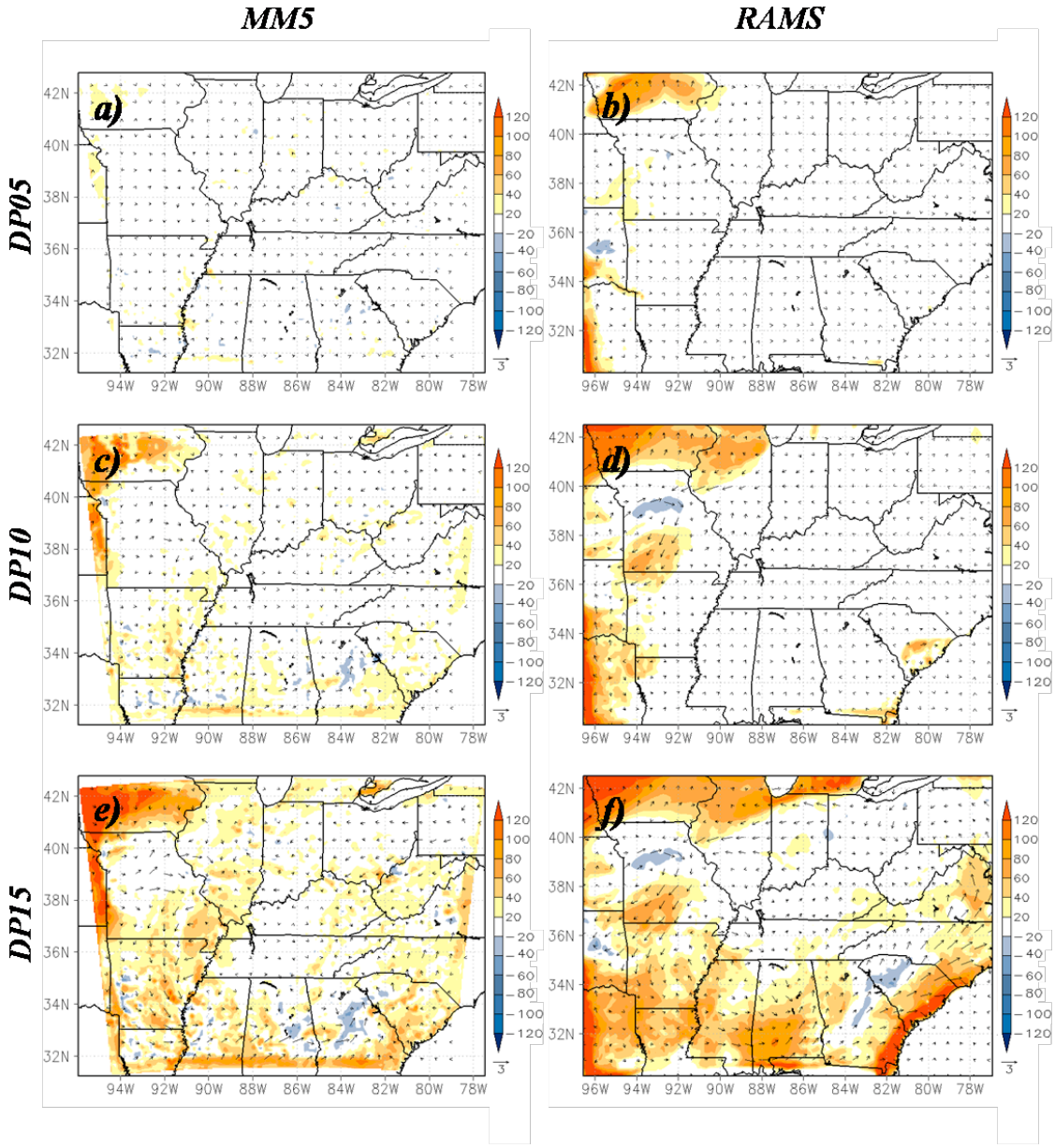

Figure 33. MM5 and RAMS dry experiment minus CTRL of 12-h averaged sensible heat fluxes (shaded according to scale, 40 m) and horizontal wind velocities (vector, 3 ms^{-1}) centered at 0000 UTC on 23 June.

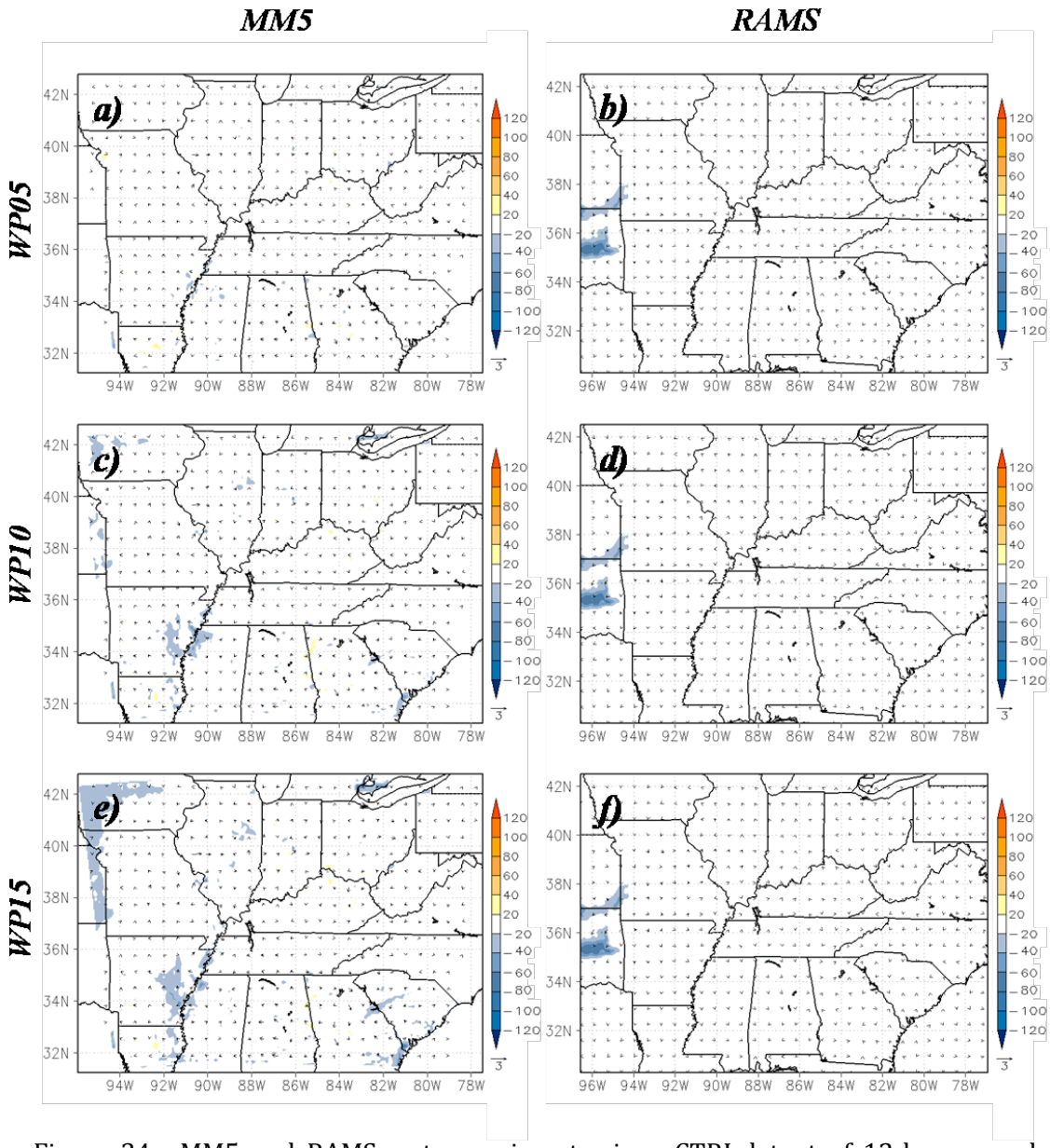

Figure 34. MM5 and RAMS wet experiment minus CTRL latent of 12-h averaged sensible heat fluxes (shaded according to scale, 40 m) and horizontal wind velocities (vector, 3 ms^{-1}) centered at 0000 UTC on 23 June.

CTRL captured the displacement of the CTRL maxima southwestward. This displacement was located over the region where the precipitation maximum for DP10 and DP15 was relocated. On the other hand, increases in SM resulted in small differences between the experiments and CTRL. WP05, WP10, and WP15 positioned sensible heat fluxes minima of -100 Wm^{-2} over western Oklahoma. Overall, wet experiments did not varied significantly with respect to each other.

CHAPTER 4

CONCLUDING REMARKS

Based on Quintanar et al. (2008) findings, our study examined and assessed the efficacy of two mesoscale models due perturbed soil moisture conditions. The study was conducted using RAMS and MM5 coupled with LEAF2 and Noah-LSM respectively. Three synoptic events were examined for June of 2006. The events presented varying synoptic forcing which ranged from weak to strong for 21-22 June, 11-12 June, and 17-18 June, respectively. The suite of experiment for both mesoscale models consisted of six single deterministic simulations in which volumetric soil moisture was increased (wet) and decreased (dry) from 0.05 to 0.15 m^3m^{-3} every 0.05 m^3m^{-3}. Precipitation accumulation and distribution, $\theta_{e,}$ vertical wind velocities, and latent and sensible heat fluxes were examined for each event.

Each CTRL simulation was compared with respect to NARR in order to assess the efficacy of each mesoscale model when simulating precipitation. RAMS simulated precipitation accumulation and distribution more accurately for the June 11-12 event. However, for 17-18 June and 22-23 of June MM5 was able to better

resolve precipitation maxima. Both mesoscale models were able to capture the warm and cold air advection which characterized the event. In addition, MM5 and RAMS also simulated the cyclonic circulation observed on 22-23 June.

Overall, the findings were consistent with Quintanar et al. (2008) study. Increases in the initial conditions of SM resulted in increased precipitation for all three events. Dry experiments presented the greatest variability of precipitation accumulation and distribution with respect to CTRL for both RAMS and MM5, with the exception of 11-12 June event. RAMS wet and dry experiments displaced the precipitation maxima with respect to CTRL for the 17-18 and 22-23 June events. This was conducive of varying 2-m horizontal wind velocities around the strongest regions of displacement. MM5 simulations also revealed more discrete displacement of precipitation maxima for the 11-12 and 17-18 June.

Negative perturbations of SM resulted in increased θ_e for MM5 experiments. The θ_e differences maxima between the experiments and CTRL were located at 700 hPa. Overall, decreases of SM did not produced significant variations of θ_e near the surface for MM5 dry experiments. Increases of SM resulted in increased θ_e near the surface by up to 2 K. RAMS DP experiments, however, produced significant increases of θ_e near the surface between 94°W and 91°W longitude for the 11-12

and 22-23 June with respect to CTRL. This maximum was coupled with lower θ_e values at the higher levels. Over the same region, RAMS wet experiments resolved lower θ_e for 11-12 and 22-23 June.

Overall, decreases in SM were conducive of increased vertical wind speeds. This was observed in both mesoscale models for all three events examined. However, moderate increases of SM of 0.05 m^3m^{-3} also produced increased vertical wind speeds. This phenomenon was also observed for all events and for both mesoscale models. In addition, latent and sensible heat fluxes were as expected. Increases in SM resulted in increased latent heat flux and decreased sensible heat flux. Both variables were able to capture the precipitation displacement revealing sharp gradients in these regions.

Positive perturbation of SM produced moderate response with respect to CTRL for all events. The aforementioned was assumed to be a result of the initial condition of SM. During each event, the initial conditions of SM were relatively high ranging from 28 to 36 m^3m^{-3} for most of the domain (not shown). Given the averaged field capacity through the region, SM maximum was established at 0.42 m^3m^{-3}. Thus increases beyond this threshold were ignored by the models. On the other hand, negative perturbations allowed the soil to become drier, further

affecting the response of the models. In conclusion, $\theta_{e,}$ vertical wind velocities, and latent and sensible heat fluxes were found to be good indicative of precipitation accumulation and displacement.

REFERENCES:

Aligo, E. A., W. A. Gallus, and M. Segal, 2007: Summer rainfall forecast spread in an ensemble initialized with different SM analyses. *Weather and Forecasting*, 22, 299–314.

Alonge, C. J., K. I. Mohr, and W. K. Tao, 2007: Numerical studies of wet versus dry soil regimes in the West African Sahel. *Journal of Hydrometeorology*, 8, 102–116.

Baker, R. D, B. H. Lynn, A. Boone, W. T. Tao, J. Simpson, 2001: The influence of SM, coastline curvature, and land-breeze circulation on sea-breeze-initiated precipitation. *Journal of Hydrometeorology,* 2, 193-211.

Baik, J, M. deMaria, and S. Rahman, 1991: Tropical cyclone simulations with the Betts convective adjustment scheme. Part III: Comparisons with the Kuo convective parameterization. *Monthly Weather Review,*119, 2889-2899.

Beljaars, A. C. M., P. Viterbo, M. J. Miller, and A. K. Betts, 1996: The anomalous rainfall over the United States during July 1993: Sensitivity to land surface parameterization and SM anomalies. *Mon. Wea. Rev.*, 124, 362-383.

Betts, A. K., J. H. Ball, A. C. M. Beljaars, M. J. Miller, and P. A. Viterbo, 1996: The land surface-atmosphere interaction: A review based on observational and global

perspectives. *Journal of Geophysical Research*, 101, 7209–7225.

Chen, C., and W. R. Cotton, 1987: The physics of the marine stratocumuluscapped mixed layer. *Journal of the Atmospheric Sciences*, 44, 2951-1977.

Chen, F., and J. Duhia, 2001: Coupling and advanced land surface-hydrology model with the Penn State-NCAR MM5 modleing system Part I: model implementation and sensitivity. *Monthly Weather Review.* 129, 569-585.

Cotton, W. R, R. A. Pielke, R. L Walko, G.E. Liston, C.J. Tremback, H. Jiang, R.L McAnelly, J. Y. Harrington, M.E. Nicholls, G.G. Carrio, and J. P. McFadden, 2003: RAMS 2001: Current status and future directions. *Meteorology and Atmospheric Physics.* 82, 5-59.

Douglas, E. M, A. Beltran-Przekurat, D. Niyogi, R. A. Pielke Sr., and C. JVorosmarty, 2008: The impact of agricultural intensification and irrigation on land-atmosphere interactions and Indian monsoon precipitation-A mesoscale modeling perspective. *Global and Planetary Change.* (in press)

Douville, H, F. Chauvin, and H. Broqua, 2001: Influence of SM on the asian and African Monsoons. Part I: Mean monsoon and daily precipitation. *Journal of Climate,* 14, 2381-2403.

Dudhia, J., 1989: Numerical study of convection observed during the winter

monsoon experiment using a mesoscale two-dimensional model. *J. Atmos. Sci.,* 46, 3077–3107.

Ek, M. and A. A. M. 2 Holstag 2004: Influence of SM on boundary layer development. *Journal of Hydrometeorology*, Vol. 5, 86–99.

__, M. and L. Mahrt, 1994: Daytime evolution of relative humidity at the boundary layer top. *Monthly Weather Review*, Vol. 122, 2709–2721.

Eltahir, E. A. B, 1998: A SM-rainfall feedback mechanism. Theory and observations. *Water Resources Research,* 34, 765-776.

Fennessy, M. J. and J. Shukla, 1999: Impact of initial soil wetness on seasonal atmospheric prediction. *Journal of Climate.* 12, 3167-3180.

Findell, K. L, and E. A. B. Eltahir, 2003: Atmospheric controls on SM-boundary layer interactions. Part I: Framework development. *Journal of Hydrology,* 4, 552-569.

Houser, P. R, W. J. Shuttleworth, J. S. Famiglietti, H. V. Gupta, K. H. Syed, and D. C. Goodrich, 1998: Integration of SM remote sensing and hydrologic modeling using data assimilation. *Water Resources Research,* 34, 3405-3420.

Kain, J. S., and M. Fritsch, 1993: Convective parameterization for mesoscale models: The Kain-Fritsch scheme. *The Representation of Cumulus Convection in*

Numerical Models, Meteor. Monogr., No. 24, Amer. Meteor. Soc., 165–170.

____, J., 2004: The Kain-Fritsch convective parameterization: An update. *Journal of Applied Meteorology*, Vol. 43, 170–181.

Kao, C-Y, and J. Bossert, 1992: Numerical simulation of an idealized convective system: comparison between parameterized and explicit resolved clouds. *Second Atmospheric Radiation Measurement (ARM) Science Team Meeting.* Technical Session, Oct 26-30

Kuo, H. L., 1974: Further studies of the parameterization of the influence of cumulus convection on large-scale flow. *J. Atmos. Sci*., **31**, 1232–1240.

___, Y-H, R. J. Reed, and Y. Liu, 1997: The ERICA IOP 5 storm. Part III: mesoscale cyclogenesis and precipitation parameterization. *Mon. Wea. Rev.*, 124, 1409-1434.

Leeper, R., R. Mahmood, A. I. Quintanar, 2009: Near-surface atmospheric response to simulated changes in land-cover vegetation fraction, and soil moisture over Western Kentucky. *Publications in Climatology*, 62, 41-

Luo, Y, E. H. Berbery, and K. E. Mitchell, 2005: The operational Eta model precipitation and surface hydrologic cycle of the Columbia and Colorado Basins. *Journal of Hydrometeorology,* 6, 341-370.

Messinger, F, G. DiMego, E. Kalnay, P. Shafran, W. Ebisuzaki, D. Jovic, J. Woollen, M. Ek, Y. Fan, R. Grumbine, W. Higgins, H. Li, Y. Lin, K. Mitchell, D. Parrish, E. Rogers, W. Shi, 2004: NCEP North American Regional Reanalysis. Paper P1.1 in 15th Symposium on Global Change and Climate Variations, Combine Preprints CD-ROM, American Meteorological Society, Seattle, WA, 11-15 January.

Mitchell, K., M. Ek, Y. Lin, F. Messinger, G. DiMego, P. Shafran, D. Jovic, W. Ebisuzaki, W. Shi, Y. Fan, J. Janowiak, J. Schaake, 2004: NCEP completes 25-year North American Reanalysis: precipiataion assimilation and land surface are two hallmarks. GEWES News, 14, 9-12.

Motovilov, Y. G, L. Gottschalk, K. Engeland, and A. Rodhe, 1999: Validation of a distributed hydrological model against spatial observation. *Agricultural and Forest Meteorology.* 98-99, 257-277.

Ookouchi, Y, M. Segal, R. C. Kessler and R. A. Pielke, 1984: Evaluation of SM effect on the generation and modification of mesoscale circulation. *Monthly Weather Review*, 112, 2281-2292.

Pal, J. S. and E. A. B. Eltahir, 2001: Pathways relating SM conditions to future summer rainfall within a model of the land-atmosphere system. *Journal of*

Climate, 14, 1227–1242.

Patra, P. K, M. S. Santhanam, K. V. J. Potty, M. Tewari and P. L. S. Rao, 2001: Simulation of tropical cyclones using regional weather prediction models. *Current Science,* 79, 70-78.

Pereira Fo., A. J, K. C. Crawford, and D. J. Stensrud, 1999: Mesoscale precipitation fields. Part II: hydrometeorology modeling, *Journal of Applied Meteorology*, 38, 102-125.

Pielke, R.A, W. R. Cotton, R. L Walko, C. J. Tremback, W. A. Lyoons, L. D. Grasso, M. E. Nicholls, M. D. Moran, D. A. Wesley, T. J. Lee, and J. H. Copeland, 1992: *Meteorology and Atmospheric Physics*, 49, 69-91.

_____, R. A., 2001: Influence of the spatial distribution of vegetation and soils on the prediction of cumulus convective rain. *Reviews of Geophysics*, 39, 151–177.

Pitman, A. J., G. T. Narisma, R. A. Pielke Sr., and N. J. Holbrook, 2004: Impact of land cover change on the climate of southwest Western Australia. *Journal of Geophysical Research*, 109.

Pirovano, G., I. Coll, M. Bedogni, S. Alessandrini, M. P. Costa, V. Gabusi, F. Lasry, L. Menut, and R. Vautard, 2007: On the influence of meteorological input on photochemical modeling of a severe episode over a coastal area. *Atmosphreic*

Environment, 41, 6445-6464.

Shao, Y, and A. Henderson-Sellers, 1996: Validation of SM simulation in landsurface parameterization schemes with HAPEX data. *Global and Planetary Change.* 13, 11-46.

Sutton, C., T. M Hamill, and T. T. Warner, 2006: Will perturbing SM improve warm-season ensemble forecasts? A proof of concept. *Monthly Weather Review*, Vol. 134, 3174–3188.

Tremback, C. J., 1990: Numerical simulation of a mesoscale convective complex: model development and Numerical results. Ph.D. Dissertation, Atmos. Sci. Paper No. 465, Department of Atmospheric Science, Colorado State University, CO 80523, 247 pp.

——, R. L. Walko, and M. J. Bell, cited 2002: RAMS/HYPACT Evaluation and Visualization Utilities (REVU) user's guide, version 2.3.1. [Available online at http://www.atmet.com/html/docs/revu/2.3.1/revupug-2.3.1.htm.]

Quintanar, A. I., R. Mahmood, J. Loughrin, and N. C. Lovanh, 2008: A coupled MM5-NOAH land surface model-based assessment of sensitivity of planetary boundary layer variables to anomalous SM conditions. *Physical Geography*. 29, 54-78.

Quintanar, A. I. R. Mahmood, M. V. Motley, J. Yan, J. Loughrin, N. Lovanh, 2009: Simulation of boundary layer trajectory dispersion sensitivity to soil moisture conditions: MM5 and Noah-based investigation. *Atmospheric Environment*. 43, 3775-3785.

Saleeby, S. M, and W. R. Cotton, 2004: Simulation of the North American monsoon system. Part I: Model analysis of the 1003 monsoon season. *Journal of Climate*, 17, 1997-2018.

Weaver, C. P, 2004: Coupling between large-scale atmospheric processes and mesoscale land-atmosphere interactions in the U.S. Southern Great Plains during summer. Part I: Case studies. *Journal of Hydrometeorolgy,* 5, 1223-1246.

Walko, R, L. E. Band, J. Baron, T. G. F. Kittel, R. Lammers, T. J. Lee, D. Ojima, R. A. Pielke, C. Taylor, C. Tague, C. J. Tremback, and P. L. Vidale, 2000: Coupled atmosphere-biophysics-hydrology models for environmental modeling. *Journal of Applied Meteorology.* 39, 931-944

Yang, M., F. Chien, and M. Cheng, 2000: Precipitation parameterization in a simulated mei-yu front. *TAO*, 11, No 2, 393-422.

Zhong, S., and J. Fast, 2003: An evaluation of the MM5, RAMS, and Meso-Eta models

at sub-kilometer resolution using VTMX field campaign data in the Salt Lake Valley. *Mon. Wea. Review.*, 131, 1301-1321.

APENDIX 1: RAMSv4.4 LEAF2 source code modifications

```
do k= 1,nzg
          nsoil = nint(gsf(i,j,k,ipatch))

   if(schar(i,j,1,1).gt.0.80) then

! If percent water > 80%, set wgp to saturation value
! wgp(i,j,k,ipatch)=slmsts(nsoil)

      elseif(k.le.4) then
if (wgptemp4(i,j).gt.slmsts(nsoil))then
wgptemp4(i,j)=slmsts(nsoil)
endif
          wgp(i,j,k,ipatch) = (wgptemp4(i,j))

      elseif(k.eq.5.or.k.eq.6.or.k.eq.7) then
if (wgptemp3(i,j).gt.slmsts(nsoil))then
wgptemp3(i,j)=slmsts(nsoil)
endif
          wgp(i,j,k,ipatch) = (wgptemp3(i,j))

elseif(k.eq.9.or.k.eq.8) then
if (wgptemp2(i,j).gt.slmsts(nsoil))then
wgptemp2(i,j)=slmsts(nsoil)
endif
          wgp(i,j,k,ipatch) = (wgptemp2(i,j))

      elseif(k.eq.10.or.k.eq.11) then
if (wgptemp1(i,j).gt.slmsts(nsoil))then
wgptemp1(i,j)=slmsts(nsoil)
endif
          wgp(i,j,k,ipatch) = (wgptemp1(i,j))

end if

! For persistent wetlands (bogs, marshes, fens, swamps), initialize with
          if (nint(schar(i,j,11,ipatch)) .eq. 31 .or. &
             nint(schar(i,j,11,ipatch)) .eq. 32) then
            wgp(i,j,k,ipatch) = slmsts(nsoil)
```